Camila Beli Silva

Development of a stable diode laser system for cavity-assisted matter-wave interferometry

Brazil

2020

Camila Beli Silva

Development of a stable diode laser system for cavity-assisted matter-wave interferometry

Dissertation presented to the Graduate Program in Physics at the Departamento de Física, Universidade Federal de São Carlos, to obtain the degree of Master in Science.

Universidade Federal de São Carlos

Departamento de Física

Programa de Pós-Graduação em Física

Supervisor: Prof. Dr. Romain M. Bachalard

Co-supervisor: Prof. Dr. Philippe W. Courteille

Brazil

2020

Aos meus pais.

Acknowledgements

I would like to thank Prof. Dr. Philippe W. Courteille for allowing me to work in this project under his supervision and for all opportunities that he gave to me during this project. I also would like to thank Prof. Dr. Romain Bachalard for taking care of the bureaucracies and for sharing your theoretical knowledge in atomic physics.

I would like to express my deepest gratitude to Prof. Dr. Raul Celestrino, who I consider as my second advisor. Thank you for your help since my first day in the lab as an undergrad student. Thank you for everything that you taught to me, all the discussions about physics and experimental things. Furthermore, thank you for your disposal to read this dissertation and for your contributions while I was writing it.

I would like to acknowledge Dr. Hans Keßler, who taught me every experimental detail of the Sr2 project. This gave me the basic experience that I needed to be able to continue working in his absence.

I also would like to acknowledge Michelle Moreno, who was my co-worker for most of this project. Thank you for being at my side, facing together all the experimental problems that arose during these two years. Thank you for the hard work and your friendship, we were a great team.

Many thanks to Prof. Dr. Rodrigo Shiozaki for every discussion, from physics to politics. I learned a lot from you. Thank your friendship, your patience and for helping me every time that I needed.

Thanks for all my colleagues from Strontium 1,2 e 3. The daily lab routine was more fun with your friendships.

I would like to thanks to Luan, Natália and all my housemates that I had during the period of this project. Thank you all for your love, friendship, support and for keeping me motivated in several aspects of my life. Life is prettier when we have such great and lovely people around us.

Also, I would like to thanks my parents, Rosilene and Edson, for always supporting me, even though they do not have an idea what I'm doing. Thank you for all your sacrifices for me to keep on this path. Without them, I would not be able to conquer things that we were not even able to dream about.

There are so many people that were really important to me during this journey. However, I'm not able to mention everybody but I'm really thankful to each one.

Lastly, I would like to express my gratitude to the Universidade Federal de São

Carlos, Universidade de São Paulo, to CAPES, CNPq and FAPESP for the financial support.

This project was realized with the support of Coordenação de Aperfeiçoamento de Pessoal de Nível Superior - Brasil (CAPES) - Financial Code 001.

Abstract

This project is part of an experiment that has been developed to probe the dynamics of ultracold strontium atoms in a vertical one-dimensional optical lattice sustained by a ring cavity. A fundamental part of the experiment is the achievement of a laser system with high-frequency stability and narrow linewidth. This dissertation explores the control of the phase and frequency of the radiation emitted by diode laser, which are essential devices of most atomic physics experiments. Phase and frequency control is achieved by electronic feedback systems, such as the Pound-Drever-Hall technique (PDH), optical phase-locked loops (OPLL) and injection locking. The basic principles and application of these locking methods are presented.

Keywords: Diode lasers. Laser lock. Frequency stability.

Abstract

Este projeto faz parte do experimento que tem sido construído com o propósito de monitorar de forma não destrutiva a dinâmica de átomos de estrôncio ultrafrios submetidos à uma rede ótica vertical sustentada em uma cavidade anelar. Uma parte fundamental para o experimento é a realização de um sistema de lasers de alta estabilidade em frequência e estreita largura de linha. Essa dissertação explora o controle de fase e frequência de lasers de diodo, os quais são os instrumentos básicos para a maioria dos experimentos de física atômica. Controle de fase e frequência são alcançados através de circuitos eletrônicos de *feedback*, como a técnica Pound-Drever-Hall (PDH), *optical phase-locked loops* (OPLL) e *injection locking*. Os princípios básicos e aplicações destes métodos de travamento de frequência são apresentados.

Palavras-chave: Laser de diodo. Travamento de laser. Estabilização de frequência.

List of Figures

Contents

1 Introduction

Techniques for non-destructive *'in-loco'* monitoring of the dynamics of a matter-wave have great potential for improving matter-wave interferometry. Applied, for example, to a Bose-Einstein condensate subjected to a periodic potential plus a uniform force, such techniques could record Bloch oscillations continuously with a single condensate. Consequently, the strong force can be measured with better time resolution, since the process of generating new condensates can be avoided (3, 4, 2, 5).

Most imaging techniques monitor the trajectory of an atomic cloud by taking snapshots at different stages of its evolution via single shots of the incident probe light. Unfortunately, the radiation pressure exerted by the probe light destroys the coherence of the matter-wave due to light scattering in all directions and the resulting photonic recoil received by the atom. This holds for techniques that measure either the instantaneous density distribution (e.g. time-of-flight imaging), or the velocity distribution, such as recoil-induced resonance spectroscopy (6) or Bragg spectroscopy (7). Very few non-destructive techniques have been demonstrated so far. Dispersive imaging (8) permitted the collection of dozens of pictures of a Bose-condensate before destruction. Electron beam imaging (9) is another example of a non-invasive mapping of ultracold atomic density distributions.

A different approach makes use of optical cavities to steer the scattered light into a single cavity mode by making use of the very large Purcell factor of resonant cavities. Hence, the scattering process becomes coherent, which makes the mechanical impact of the incident light predictable, while heating can be avoided. The dynamics have been experimentally demonstrated using a ring cavity (10, 11). If one of two counter-propagating cavity modes was pumped by a sufficiently far-detuned laser, the Bose-condensate could only respond by scattering light into the backward direction. The time-evolution of the recorded backscattered light contains all information on the condensate's trajectory. This feature can be harnessed to monitor predefined matter-wave trajectories, for example, Bloch oscillations (4, 2).

Ultracold strontium is a suitable candidate in matter-wave interferometry for several reasons. It presents a strong dipole-allowed transition (32 MHz linewidth) and a narrow intercombination line (7.6 kHz linewidth) that allows rapid optical cooling down to almost recoil temperature. The electronic ground state ($^1S_0$) has no magnetic moment, which makes it insensitive to stray magnetic fields. The abundant ^{88}Sr isotope exhibits a small scattering length (-2a_B), such that interatomic collisions can be neglected.

The goal of this project is to build a spectrally stable and narrow laser system at the frequency of the strontium intercombination line that will be used to cool down the

atoms close to the recoil temperature. Moreover, it will be shown how to stabilize the frequency and phase of a laser that will provide the light for a one-dimensional optical lattice sustained by a ring cavity, where the atoms shall perform Bloch oscillations, and also the light to probe the atomic dynamics. This is the first step towards the implementation of a gravimeter based on a coherent matter-wave.

1.1 Atomic Interferometry Gravimeter

In analogy with optical interferometers, ultracold atomic matter-waves, a Bose Einstein Condensate (BEC) for example, can be divided and recombined, giving rise to atomic interference signals (12). Ramsey sequence of optical pulses transfer momentum to parts of the matter-wave, allowing in this way, interferometers such as Mach-Zehnder or Ramsey-Bordé to be used as gravimeters, when applied to matter-waves freely evolving under the influence of gravity. (13). Measurements of gravitational acceleration with sensibility of 2×10^{-7} m/s^2 with 1 s of integration time and precision around 1×10^{-9} m/s^2 were achieved (14).

Higher precisions can be reached with a longer integration time. However, standard procedures are limited by slow repetition rates since the test mass needs to be elevated in the field of gravity before being released, which takes a finite time. To avoid this process, it is necessary to use non-destructive techniques to measure the motional state of an atomic cloud. A proposed way for implementing this idea consists of continuous monitoring of the atomic velocity of ultracold atoms that undergo Bloch oscillations in a one-dimensional optical lattice subjected to the gravitational force. The instantaneous atomic velocity can be measured exploiting an effect, termed CARL (collective atomic recoil lasing), where light is coherently back-scattered by moving atoms into one of the modes of a ring cavity (2).

1.1.1 Collective atomic recoil laser

The collective atomic recoil laser (CARL) was first predicted in 1994 (15) as an atomic analog of the free-electron laser (FEL) since it converts atomic momentum into coherent radiation. The model is based on two-level atoms driven by two counterpropagating light fields: a pump laser beam from an external source and a copropagating probe beam, spontaneously generated by the atoms.

To understand the mechanism more easily lets first consider two counterpropagating waves of modes ω_α and ω_p red-detuned from the atomic resonance. Initially, the two frequencies are equal and form a standing wave where the atoms are placed at the antinodes by dipolar force. An atom can absorb a photon from the mode ω_p and re-emit it into the ω_α. In this process, the atom exchanges its momentum by $2\hbar k$. Since the atom

has a certain velocity v, the emitted photon is Doppler-shifted by kv and mixes into the mode ω_α. This results in a phase shift of the standing wave that now starts to move. The displacement of the standing wave modifies the potential energy of other atoms. As a consequence, for a sufficiently cold atomic ensemble, the momentum of the atoms begin to evolve in time. Both degrees of freedom, the phase of the standing wave and the atomic motion, self-synchronize in this process.

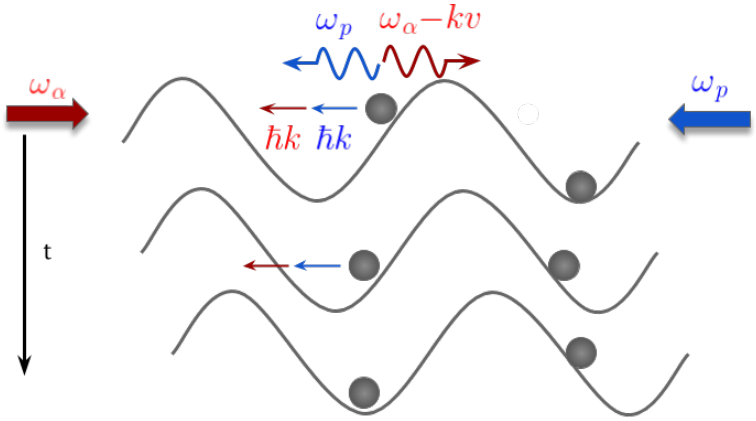

Figure 1 – The atom on the left is initially placed on the slope of the standing wave. When it is accelerated towards the bottom of the potential, it pushes the standing wave to the right. The atom placed initially at the valley of the potential is then granted with potential energy and starts to oscillate.

The backaction of an atom onto the phase of the standing light wave is very weak. To detect it, it is necessary to have many atoms moving synchronously and the phase of the standing wave needs to be a free parameter. To satisfy these conditions, a high-finesse ring cavity can be used since the phase of the standing wave is not fixed by boundary conditions of the mirror surfaces. Furthermore, the counterpropagating fields in a ring cavity form separate modes carrying independent numbers of photons yelding to independent photon detection. The backscattering acts on the phase of the standing wave. Also, the atoms tend to arrange themselves being trapped by the dipolar forces at the anti-nodes of the standing wave, in which the dipole force corresponds to backscattering from one mode to the other. Under these circumstances, it allows the observation of the backaction of the atomic motion on the phase of the traveling standing wave becomes possible.

Now considering that just the mode α_p is pumped into the cavity and we want to see the evolution of the probe mode α, where $\left|\alpha_p\right|^2$ and $|\alpha|^2$ are the photon numbers. The coupling between the modes only happens in the presence of atoms due to backscattering events and is given by the single-photon light shift (2)

$$U_0 = \frac{\Omega_{sp}^2}{\Delta_a}, \tag{1.1}$$

where Ω_{sp} is the single-photon Rabi frequency and Δ_a is the detuning from the atomic resonance. We can write the mode rate equation for α as (16)

$$\dot{\alpha} = -\kappa\alpha + iNU_0\alpha_p \sum_{n=1}^{N} e^{2ikx_n}, \tag{1.2}$$

where κ is the cavity decay width, k is the wavenumber, x_n is the position of the nth atom and N the number of atoms. The first term in equation 1.2 describes the photon loss through the cavity mirror, and the second one is photon gain of α from mode α_p through backscattering. The atom at position x feels the classical potential of the stationary light wave, and therefore the dipolar force. The dynamics of the atom trough the scattering process is given by (16)

$$m\ddot{x}_n = -2i\hbar kU_0(\alpha_p\alpha^* e^{ikx_n} - \alpha_p^*\alpha e^{-ikx_n}), \tag{1.3}$$

with α and α_p, denoting the expectation values of field operators. The dipolar force is described in terms of photonic recoil through photon absorption from one mode and photon stimulated emission into the other field mode. In each event described, the atom exchanges its momentum by $2\hbar k$.

We can also define the bunching parameter that describes the atomic ordering

$$b \equiv \frac{1}{N}\sum_{n} e^{-2ikx_n}. \tag{1.4}$$

When $b = 0$, the atomic density distribution is homogeneous. The phases of back-scattered photons interfere destructively and the impact of the scatterers on the light modes cancels out. For $b = 1$, the atoms are equidistantly ordered. This means that the atoms are placed in the antinodes of the standing wave, generating a matter grating. Then, the light is efficiently Bragg scattered. The signature of CARL is the self-bunching amplification leading to an exponential growth of the counterpropagating mode.

To experimentally verify how the probe mode behaves in time, *Kruse et al.* (1) observed the beat signal between the two counterpropagating modes when just the α_p mode was pumped into the ring cavity. Since the frequency of the probe mode is Doppler-shifted, the frequency difference between the counter-propagating cavity modes is translated into variations in the amplitude of the beat signal $P_{beat} \propto \left|\alpha + \alpha_p\right|^2$.

It was also observed that the atoms copropagate with the moving standing wave. They are constantly accelerated by the light force that comes from the photonic momentum transfer. In the absence of friction, the atoms are constantly accelerated until the Doppler-shifted frequency of the back-scattered light does not fit in the cavity mode, whose finesse was very high (80000) and which, therefore, had a very narrow resonance profile. Then,

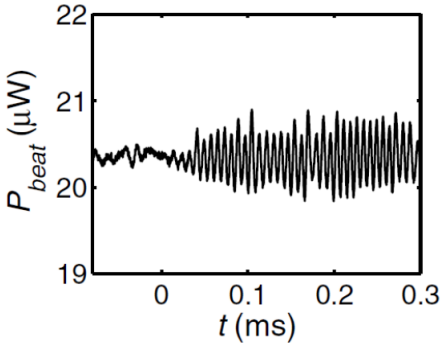

Figure 2 – Measured beat signal obtained with a unidirectionally pumped cavity. Modified from *Kruse et al.* (1) (2003).

after an inicial behavior of exponential growing, the atomic bunching and the probe mode intensity start do decrease.

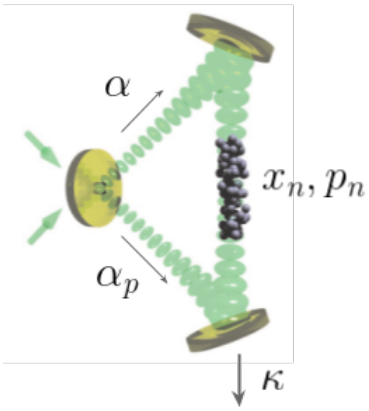

Figure 3 – Representation of ring cavity with two counterpropagating modes that are coupled in the presence of atoms.

1.1.2 Bloch Oscillations

The phenomenon of Bloch oscillations (BO) was predicted for electrons in a periodic crystal potential when a static electric field is applied (17). It was first demonstrated with electrons in semiconductor superlattices subjected to a force exerted by a DC electric field (18). Cold atoms in optical lattice have allowed an alternative realization of BOs with long coherence times (19).

To produce the BO dynamics with an atomic matter wave, we can consider two counterpropagating laser fields of equal intensity and wavenumber k_l that forms a one-dimensional optical lattice. Then, the atoms need to be subjected to a homogeneous and constant force. In our case, this force is the gravitational force. The discussion that follows

deals with the Bloch Oscillations for this particular case. We can write the time-dependent Schrödinger equation describing the motion of an atom as

$$i\hbar\frac{\partial\psi}{\partial t} = -\frac{\hbar^2}{2m}\frac{\partial^2\psi}{\partial x^2} + \frac{\hbar W_0}{2}\sin(2k_l x)\psi - mgx\psi, \tag{1.5}$$

where $\hbar W_0$ is the depth of the externally imposed optical lattice. To eliminate the gravitational term we change to the moving frame through Galilean transformation using $e^{imgxt/\hbar}$. We can expand the time-dependent wave function into plane waves (16)

$$\psi(x,t) = \sum_n c_n(t)e^{2ink_l x}\cdot e^{imgxt/\hbar}. \tag{1.6}$$

Inserting equation 1.6 into 1.5 we obtain a set of equations for the coefficients c_n,

$$\frac{dc_n}{dt} = -4i\omega_{rec}(n+\nu_b t)^2 c_n + \frac{W_0}{2}(c_{n+1} - c_{n-1}), \tag{1.7}$$

where $\omega_{rec} = \hbar k_l/2m$ is the recoil frequency and $|c_n|$ is the time-dependent probability of finding the atom in the nth momentum state $p_n = n(2\hbar k)$. The frequency of BO is given by

$$\nu_b = \frac{mg}{2\hbar k_l}, \tag{1.8}$$

where $\lambda_l = 2\pi/k_l$ is the lattice lasers wavelength and $\hbar$ is the Planck's constant. With the population of the momentum states as $|c_n|^2$,the momentum of the center-of-mass in the laboratory frame can be written as

$$\langle p\rangle_{lab}/2\hbar k_l = \sum_n n|c_n(t)|^2 - \nu_b t \tag{1.9}$$

The evolution of the momentum given by equation 1.9 above has an oscillatory behavior as illustrated in Figure 4. We can understand the matter-wave dynamics by the picture of Bragg reflection: The matter-wave is constantly accelerated and reduces its de Broglie wavelength, until a value where it is commensurable with the periodicity of the optical potential. At this point, the atoms are scattered back by Bragg reflection.

In order to enable the detection of the BO, some conditions need to be fulfilled. If the potential is too deep, it flattens the lowest band and reduces the amplitude of the oscillation, making it difficult to measure. Also, it requires a minimal force to scan the whole first Brillouin zone during the time of the experiment, which imposes a lower limit on the potential depth. Furthermore, the force must be weak enough to avoid non-adiabatic transitions between Bloch bands (20).

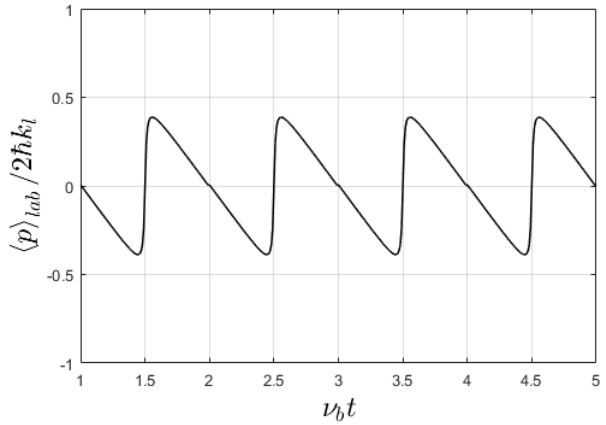

Figure 4 – Dynamics of Bloch oscillations in the laboratory reference frame.

1.1.3 Measurement of Bloch Oscillations

In experiments of BO performed with cold atoms, the measurement of the motional state of the atomic cloud is generally done by destructive techniques such absorption imaging measuring the instantaneous atomic position or velocity-selective Raman spectroscopy measuring the instantaneous atomic velocity (19, 20). Indeed, for each measurement of the actual phase of a Bloch oscillation, the atomic cloud is shattered and a new ensemble needs to be prepared, cooled, filled into the optical lattice, and then, subjected to Bloch oscillations. By varying the time evolution before detection, Bloch oscillations are reconstructed and after the acquisition of a large amount of data the acceleration force can be extracted.

The process is difficult and sensitive to uncertainties and fluctuations in the initial conditions in the preparation of the cloud, such as the number of atoms and temperature. Therefore, the detection bandwidth is limited by the repetition rate of the experimental sequence. This also means that the signal-to-noise ratio achieved within a certain time is limited. For measurements of the Earth's gravitational field, this integration time limitation is not a stern restriction. For local gravitational measurements, on the other hand, a faster response from the gravimeter is desirable.

The measurement process can be dramatically accelerated if, instead of taking successive images of the atomic position, the impact of atomic motion on the surrounding standing light wave can be monitored. This can be done by combining the Bloch oscillations with the CARL effect of atoms in a ring cavity (2). If the cavity finesse is high enough, the cavity's fields carry signatures of Bloch oscillations, which then, can be non-destructively monitored recording the light leaking through the cavity mirrors.

To describe the matter-wave dynamics combining the two effects, we can consider the system described in section 1.1.1, were ultracold atoms are placed within a high finesse ring cavity with initially just the pump mode α_p coupled to the cavity. For the atoms to

perform BO, an externally one-dimensional optical lattice aligned along the cavity axis is imposed. The gravitational force plays a role as the constant force accelerating the atoms along the same cavity axis (see Figure 5(a)). If the atomic cloud is sufficiently dilute, atomic interactions can be disregarded and we can write the equations of motion for the atomic wave function ψ and the probe mode α as

$$i\hbar\frac{\partial\psi}{\partial t} = -\frac{\hbar^2}{2m}\frac{\partial^2}{\partial x^2} + \frac{\hbar W_0}{2}sin(2k_l x)\psi - mgx\psi - i\hbar U_0(\alpha e^{2ik_l x} - \alpha^* e^{-2ik_l x})\psi \tag{1.10}$$

$$\frac{d\alpha}{dt} = -\kappa\alpha + 2k_0\alpha_p^* \int N|\psi|^2 e^{-2k_0 x}dx. \tag{1.11}$$

We can understand the atomic dynamics as follows: While the atoms perform Bloch oscillation in the externally imposed optical lattice due to the gravitational force, the CARL effect makes the atoms coherently Bragg-scatter photons from the pump mode into the probe mode provided and the atomic matter wave forms a periodic grating. This, however, is only the case at the instants of time when the atoms undergo a Bloch oscillation-induced Bragg-reflection. At those moments every atom finds itself in a superposition of two momentum states: up and down. In this way, the light scattered back by CARL is a direct signature of a Bloch oscillation.

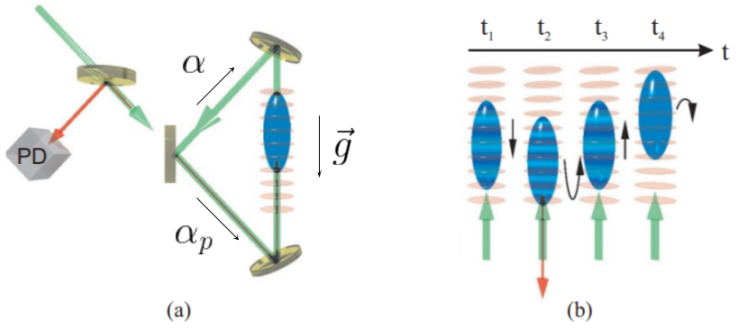

Figure 5 – (a) Scheme for continuous detection of Bloch oscillation from a matter-wave falling inside a vertical standing light wave sustained by a ring cavity. (b) Time evolution of the matter-wave dynamics.

The cooperative dynamics and synchronization between CARL and BO depend on the strength of the collective atom-field coupling. *M. Samoylova et al.* (2) observed through simulations a range of parameters that leads to regular and stable BO, where the atoms stay on the first Bloch band. The frequency of these oscillations is imprinted on the probe mode field that can be monitored by a photon leakage through the cavity mirror. This ensures a non-destructive technique to monitor the motional state of an atomic cloud, which is an important step to high precision gravimetry.

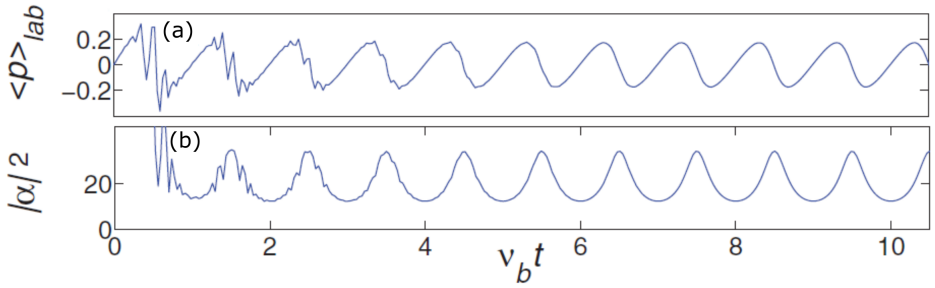

Figure 6 – Time evolution of (a) Average of the atomic momentum $\langle p \rangle_{lab}$ in the laboratory frame. (b) the average photon number $|\alpha|^2$ in the regime dominated by Bloch dynamics. Adapted from *M. Samoylova et al.* (2) (2014).

2 Laser Cooling and Trapping

Light forces are the basis of atomic position and momentum manipulation with light. These forces exerted on an atom can be conservative or dissipative. The first one is known as "dipolar force" and is often used to manipulate and trap atoms (21).

The second one is called "radiation pressure", which arises from the recoil that an atom experiences when absorbs or emits a photon. For each absorption process, a quantum momentum $\hbar k$ is transferred to the atom in the direction of the light propagation, which creates an average force in this direction. Since the spontaneous emission following an absorption occurs in random directions, the average over many cycles is zero, thus, there is no average force due to spontaneous photon emission.

The recoil associated with the emission-absorption process of photons leads to changes in the atom's velocity. These discrete velocity changes set a limit to the reachable temperature of the atomic cloud in a trap. This limit is called recoil temperature T_{rec} and is given by (21)

$$T_{rec} = \frac{\hbar^2 k^2}{2mk_B}, \tag{2.1}$$

where $\hbar$ is the reduced Planck's constant, m is the atom's mass, k_B the Boltzmann constant, $k = 2\pi/\lambda$ is the wave vector of the light field and λ the corresponding wavelength.

Those forces and their use for optical cooling and atomic manipulation is largely discussed in the literature (21, 22). In this chapter some aspects of it will be discussed.

2.1 Optical molasses

In the Doppler cooling model, we treat the action of optical forces quantitatively considering the amplitude, phase and frequency of a classical radiation field that interacts with a two-level atom.

For a two-level atom that is radiated by a light field, if there's atom-light coupling, the atomic population is going to oscillate between the two atomic levels involved in that atomic transition. This population oscillation is characterized by the Rabi frequency Ω, which is proportional to the dipole moment d, that characterizes the strength of the atom-light coupling and to the amplitude of the light's electric field $\mathbf{E}_0$

$$\Omega = \frac{\mathbf{d} \cdot \mathbf{E}_0}{\hbar}. \tag{2.2}$$

The coupling dipole moment and the vacuum field yields the spontaneous decay rate for the transition (21)

$$\Gamma = \frac{\omega_0^2}{3\pi\epsilon_0\hbar c^3}|d|^2\,, \tag{2.3}$$

where ϵ_0 is the permittivity of free space and c is the speed of light in vacuum. We can define the saturation parameter as

$$s = \frac{I}{I_s} = \frac{\Omega^2}{\Gamma^2/2}, \tag{2.4}$$

where I is the peak intensity of the incident beam and I_s is the saturation intensity for a given atomic transition.

The average force that the photon absorption produces on the atoms is the rate of absorbed photons γ_p times the photon momentum (23)

$$\langle \mathbf{F} \rangle = \hbar \mathbf{k} \gamma_p, \tag{2.5}$$

where

$$\gamma_p = \frac{\Gamma}{2}\frac{s}{1 + s + (2\Delta/\Gamma^2)^2}, \tag{2.6}$$

with $\Delta = \omega - \omega_0$ is the detuning from the atomic resonance ω_0. Considering now that the atom is moving in z direction with velocity v_z towards the light field. The total detuning including the Doppler shift seen by the atom will be

$$\Delta \to \Delta + kv_z. \tag{2.7}$$

Now, for two light fields propagating in $\pm z$ direction, the total force experienced by the atom is given by $\mathbf{F} = \mathbf{F}_+ + \mathbf{F}_-$, where

$$\mathbf{F}_\pm = \pm\hbar\mathbf{k}\frac{\Gamma}{2}\frac{s}{1 + s + 4(\Delta \mp kv_z)^2/\Gamma^2}. \tag{2.8}$$

If $|kv_z|$ is small compared to Γ or to $|\Delta|$, by Taylor expansion in the velocity v_z, we have

$$F_z \simeq 4\hbar k s \frac{kv_z(2\Delta/\Gamma)}{(1 + (2\Delta/\Gamma)^2)^2}. \tag{2.9}$$

For a red-detuned light, i.e., $\Delta < 0$ the cooling force will be opposed to the atomic motion and proportional to its velocity, acting as a damped harmonic oscillator. Now, for

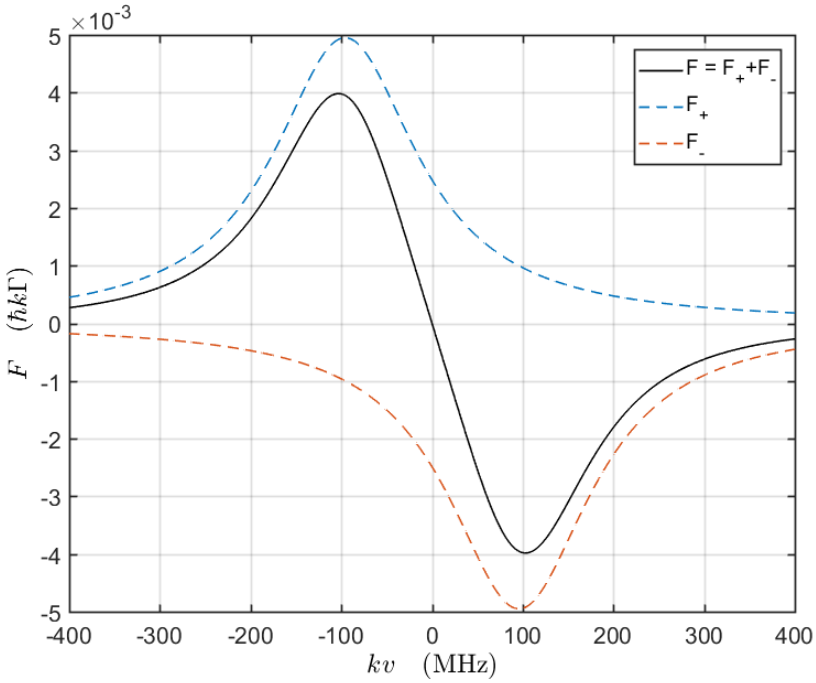

Figure 7 – Molasses force as a function of the atom's velocity. For low velocity, it is approached by a linear dissipative force behavior.

three-dimensional cooling, 6 counter-propagating beams are required. Then, we can define the the friction coefficient due to the contribution of all beams

$$\alpha = -4\hbar k^2 \frac{s(2\Delta/\Gamma)}{(1+s+(2\Delta/\Gamma)^2)^2} \tag{2.10}$$

2.1.1 Doopler cooling limit

We can rewrite equation 2.5 for the limit of low intensity $I/I_s \ll 1$, and also for the approximation for low velocity $|kv| \ll \Gamma, |\Delta|$

$$F = 4\hbar k \frac{kv(2\Delta/\Gamma)}{\left[1+(2\Delta/\Gamma)^2\right]^2} \frac{I}{I_s}. \tag{2.11}$$

The damping force present in the optical molasses leads to a cooling rate of

$$\left(\frac{dE}{dt}\right)_{cool} = Fv. \tag{2.12}$$

Since each cycle of absorption followed by spontaneous emission can happen in random directions, this represents a random fluctuation in momentum space which produces heating. We now consider the total photon scattering rate R, which is given by γ_p in the

limit of $I/I_s \ll 1$, the heating rate is (23)

$$\left(\frac{dE}{dt}\right)_{heat} = \frac{\hbar^2 k^2 R}{m} = \frac{\mathcal{D}_p}{m}, \tag{2.13}$$

where $\mathcal{D}_p$ is the momentum diffusion constant and m the atomic mass. Using the same low-velocity approximation as before, we have

$$\left(\frac{dE}{dt}\right)_{heat} = \frac{\hbar^2 k^2}{m} \frac{\Gamma}{1 + (2\Delta/\Gamma)^2}. \tag{2.14}$$

At some point, the Doppler cooling rate will be balanced by the heating leading to a velocity equilibrium. We can interpret this as the final average velocity of the atoms that are subjected to the cooling process, i.e., the average velocity of the atomic cloud. That is, the kinetic energy Mv_{rms}^2 can be associated with the thermal energy $k_B T/2$, and we can get an expression for the temperature of the atomic cloud

$$T = \frac{\hbar\Gamma}{2k_B} \frac{1 + (2\Delta/\Gamma)^2}{2|\Delta|\,\Gamma}. \tag{2.15}$$

The temperature has minimum value for $\Delta = -\Gamma/2$, which is known as the Doppler temperature limit T_D

$$T_D = \frac{\hbar\Gamma}{2k_B}. \tag{2.16}$$

To expand this analysis for the tridimensional case, we need to include in equation 2.11 the contribution of the 6 counterpropagating beams leading to a total light intensity of $I/I_s \to 6I/I_s$. Also, instead of considering the approximation of low intensity for the scattering rate R, we now take the γ_p. With these conditions, the equilibrium temperature becomes

$$T = \frac{\hbar\Gamma}{8k_B} \frac{1 + 6I/I_s + 4(\Delta/\Gamma)^2}{|\Delta|\,/\Gamma}. \tag{2.17}$$

In this expression, we can see how temperature depend on the intensity of the incident radiation.

2.2 Magneto-Optical Trap (MOT)

The optical molasses leads to a cooling of the atoms but does not confine them in space. In order to trap the atoms while the cooling process happens, we make use of a magnetic field that induces spacially dependent Zeeman shifts. We consider a two-level

atom with total angular momentum J=0 and J=1, in the ground and excited states, respectively, that travels along the z-direction. When we apply a magnetic field $B(z)$ that increases linearly with the distance from the origin, the Zeeman shift for the $m_j = \pm 1$ magnetic sublevel of the excited state increases, which is given in units of frequency by (16)

$$\Delta_B = \frac{\mu_B g_j m_j}{\hbar} \frac{dB_z}{dz} z = \pm \mu \partial B_z z, \tag{2.18}$$

With $\frac{dB_z}{dz} = \partial B_z$, $\mu = \mu_B g_j m_j / \hbar$, where μ_B is the Bohr magneton constant, g_j is the Landé g-factor and m_j is the quantum number associated to the magnetic moment in the direction of the magnetic field.

When shining a red-detuned laser beam in the $\pm z$ direction the equation 2.19 becomes

$$F_{\pm z} = -\hbar k \frac{\Gamma}{2} \frac{s}{1 + s + 4(\Delta \pm k v_z \pm \mu \partial B_z z)^2 / \Gamma^2}. \tag{2.19}$$

The MOT configuration exploits the spatially dependent Zeeman shift to confine the atoms. Then, it is necessary to use counter-propagating beams with opposite polarization with respect to the quantization axis. The circularly polarized σ^+ laser light tuned below resonance exerts a light force toward the center of the trap on $m_j = +1$ atoms on the left side of Figure 8 , while σ^- light exerts a light force toward the center of the trap on $m_j = -1$ atoms on the right side.

Therefore, the atoms feel a restoring force that pushes them back to the origin. The atomic motion always introduces velocity-dependent terms in the forces, but only for $\Delta < 0$ it leads to cooling. For small displacement and velocities, a Taylor expansion up to first order can be made in equation 2.19 and the total restoring force can be expressed by the sum of a term linear in velocity, and another, linear in the displacement

$$F_{MOT} = F_{1z} + F_{2z} \simeq -\alpha \dot{z} - \kappa z, \tag{2.20}$$

where α and κ play the role of friction coefficient and spring constant, respectively, as in a damped harmonic oscillator.

Atoms with Zeeman structure in the ground state can be cooled below the Doppler limit, although this does not hold for ^{88}Sr atoms, which does not possess a ground state Zeeman structure. The mechanism used to achieve this is based on spatial polarization gradients and this cooling process is called Sub-Doppler cooling (24).

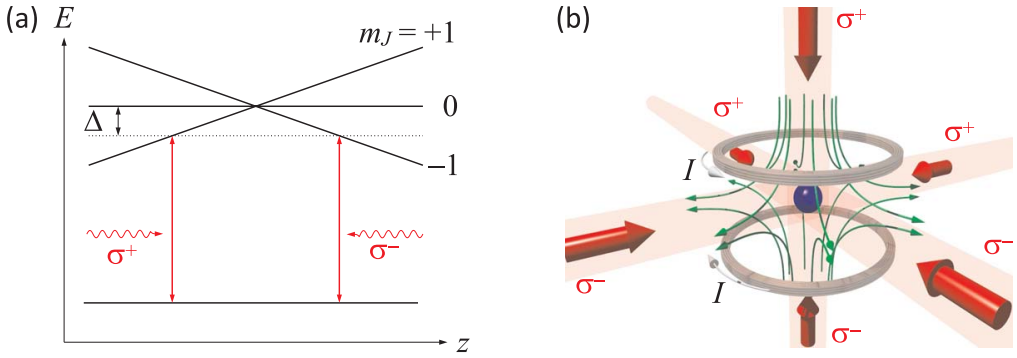

Figure 8 – (a) Energy diagram along one axis of the MOT, showing the magnetic sublevels of a $J \rightarrow J+1$ transition in the presence of a quadrupole magnetic field. (b) Three mutually orthogonal, counter-propagating pairs of laser beams are aimed at the trap center, defined by the zero of a quadrupole magnetic field created by a pair of coils in anti-Helmholtz configuration.

3 Laser cooling and trapping strontium

3.1 Strontium

Strontium (Sr) is an alkaline earth metal from group 2 or IIA of the Periodic System of Elements. It is abundant in nature in the form of sulfates and carbonates. There are four naturally occurring isotopes of Sr out of which ^{84}Sr, ^{86}Sr and ^{88}Sr are bosonic and ^{87}Sr is fermionic. The nuclear spin of all bosonic alkaline-earth elements is zero (I = 0), which leads to an absence of hyperfine structure. The nuclear spin of ^{87}Sr is I = 9/2, one of the highest of the stable alkaline-earth isotopes.

Neutral Sr atoms have 38 electrons, with two being the valence ones. In this configuration, the excited states exhibit Helium-like features. It presents singlet states, which are antissymetric upon spin exchange, and triplet states that are symmetric. The ground state of the bosonic isotopes is the singlet state $^1S_0$ which has magnetic dipole moment zero (J=0), i.e., it is insensitive to magnetic fields. There are narrow intercombination lines between singlet and triplet states, which can be used for laser cooling and as reference frequency in atomic clocks (25).

Figure 9 shows the ^{88}Sr electronic structure, and the transitions for one of the two valence electrons, while the other one remains on the $5s$ level. The transition from the ground state to $(5s5p)^1P_1$ is broad, with a linewidth of $\Gamma = 2\pi \times 32$ MHz, and it is not fully closed, since the transition $(5s^2)^1P_1 \rightarrow$(4d5s $)^1D_2$ can occur at a ratio of 1:50000, which then, decays to the states $(5s5p)^3P_1$ and $(5s5p)^3P_2$.

From the $(5s5p)^3P_1$ state, the atoms decay quickly enough to the ground state, so they are back to the cooling cycle. On the other hand, the $(5s5p)^3P_2$ state has a long lifetime. To recover these atoms, one needs to pump them into higher states, from which decay to the $(5s5p)^3P_1$ state is likely to occur. A path that can be used to achieve this is by exciting the atoms to the $(5s6s)^3S_1$ using a laser at 707 nm. Unfortunately, from this state, the atoms can also decay into $(5s5p)^3P_0$, which has a long lifetime, and thus, another laser at 679 nm is required to excite these atoms to the $(5s6s)^3S_1$ decaying to the $(5s5p)^3P_1$ state.

It is also possible to excite the $(5s5p)^3P_2$ state to $(5s6d)^3D_2$ or $(5s5d)^3D_2$ states using a 497 nm and 403 nm lasers, respectively. They can decay back into $(5s5p)^3P_2$ and be repumped again, or decay directly to the $(5s5p)^3P_1$ state.

The abundant ^{88}Sr isotope has a small scattering length ($-2a_B$) which makes it insensitive to loss of coherence by collisions. It is not surprising that very stable Bloch oscillations induced by gravity on ultracold ^{88}Sr trapped in a vertical standing wave could

be observed and applied to gravity acceleration measurement (26).

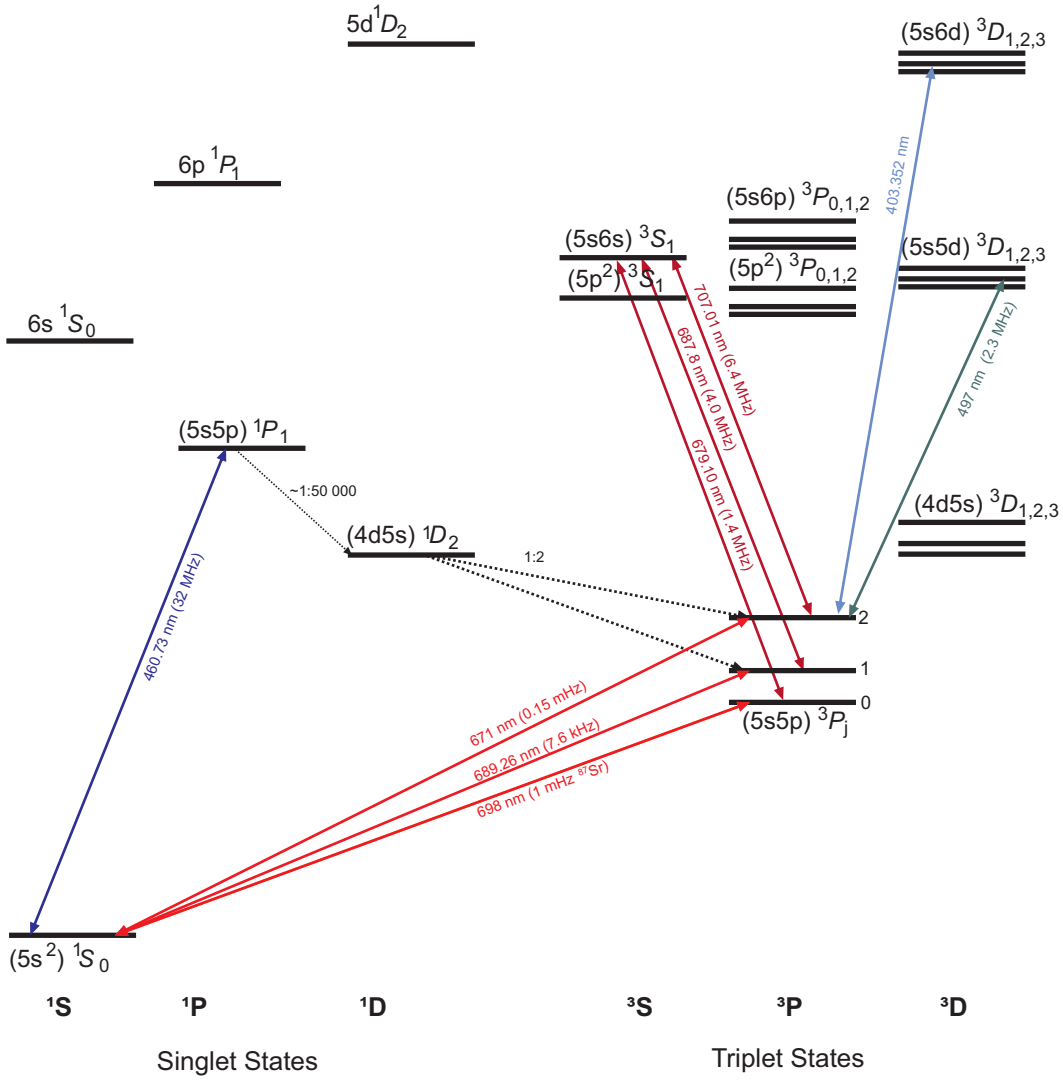

Figure 9 – Simplified ^{88}Sr electronic structure with the relevant cooling transitions and the repumping transitions that are typically used.

3.2 Broad-line MOT

Broad transitions for Doppler cooling are largely used in laser cooling experiments. A broad transition is defined by $\Gamma/\omega_r \gg 1$, where Γ is the transition natural linewidth and $\omega_r = \hbar^2 k^2/2m$ is the single-photon recoil frequency. The ^{88}Sr $^1S_0 - ^1P_1$ transition is characterized by a broad line, which has $\Gamma/\omega_r \approx 3 \times 10^3$. In this case, the Doppler temperature $T_D = \hbar\Gamma/2k_B$ sets the limit for the achievable temperature in this regime. Furthermore, gravity can be neglected since the maximum radiative force F_{rp} is much

larger than gravitaty F_g

$$F_{rp}/F_g = \frac{\hbar k \Gamma}{2mg} \approx 1 \times 10^5. \tag{3.1}$$

Where $\hbar$, k, m and g are Planck's constant, light field wave number, atomic mass and the gravitation acceleration, respectively.

For high intensities, γ_p saturates to $\Gamma/2$. For this regime, we calculate the maximum deceleration that the optical cooling can exert on the atom

$$a_{max} = \frac{\hbar k \Gamma}{2m} \simeq 9.5 \times 10^5 \ m/s^2. \tag{3.2}$$

Equation 3.2 shows the maximum accelaration for the ${}^1S_0 - {}^1P_1$ transition of ^{88}Sr atoms , which has a linewidth of $\Gamma = 2\pi \times 32$ MHz. This is an important feature that allows us to capture atoms with high velocities from a thermal source, and then, cool them down to mK temperatures in a MOT.

3.3 2D and 3D-MOT Setup

Figure 10 shows the layout of our experiment. The whole vacuum chamber fits on a 50 × 50 cm base plate. It consists of two vacuum chambers linked by a 2 cm long differential vacuum tube with 2 mm inner diameter. Combinations of ion pumps and non-evaporable getter pumps allow us to maintain a vacuum of 10^{-8} mbar in the 2D-MOT chamber and 10^{-9} mbar in the science chamber.

The 2D-MOT is loaded from a Sr dispenser (AlfaVakuo e.U.). Although there is no direct path from the dispenser to the vacuum windows, and moreover, Sr atoms tend to be quickly absorbed when colliding with the inner walls of the chamber, we have observed that a macroscopic amount eventually gets deposited on the windows, which coats them with an opaque layer. To minimize this problem, baffles are mounted around both the dispenser and the viewports, such that simple atomic trajectories towards the windows are blocked. No coating of the windows has been observed since this technique was applied.

The 2D-MOT is operated with permanent magnets arranged in a way such that the symmetry axis is magnetic field-free. We use 2 retroreflected laser beams tuned 20 MHz below the blue cooling transition at 461 nm. Each beam has 17 mW with $1/e^2$ waists of 5 mm (see Figure 9).

The atoms captured in the 2D-MOT are then subjected to a resonant 80 μW "push beam", which accelerates them towards the science chamber, where they are recaptured by a 3D magneto-optical trap called "blue MOT". The 461 nm light is generated by a frequency-doubled Ti:sapphire laser (MSquared), that is frequency locked by standard

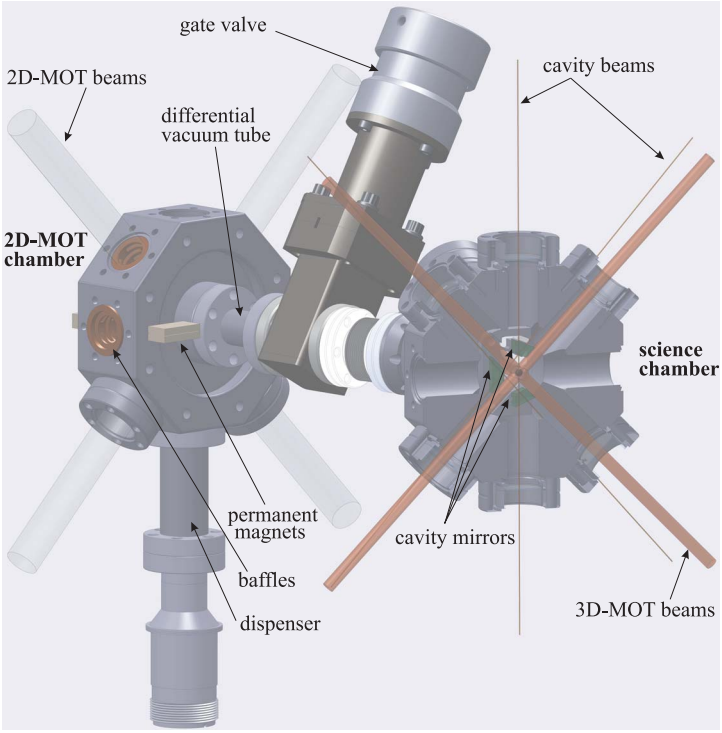

Figure 10 – 2D-MOT and science chamber setup

absorption spectroscopy. Additionally to the 2D-MOT, we have two so-called "Zeeman beams" with 10 mW each, $1/e^2$ waist of 5 mm which are tuned 150 MHz below the resonance. These extra MOT beams cool down the hottest atoms and improve the 3D-MOT atom number approximately by 20% (27).

The magnetic field in the blue MOT is generated by a pair of coils in an anti-Helmholtz configuration that produces a magnetic field gradient of 65.3 G/cm for a current of 8.75 A. The blue MOT is built in a retroreflected setup, where each of the three retro-reflected beams is tuned 15 MHz below the blue cooling transition, with 4.5 mW each and $1/e^2$ waist of 3.34 mm. Additionally, at least one repumping laser is required, which recycle the atoms pumped into the state $(5s5p)^3P_2$. Eventually, a second repumping laser is also used for recycling the atoms pumped into the metastable $(5s5p)^3P_0$ (in which some atoms fall after being repumped from the $^3P_2$). In our experiment, we have at our disposal repumping lasers at 679 nm and 707 nm.

The fully description and characterization of the "Blue System", 2D and 3D-MOT can be found in (27).

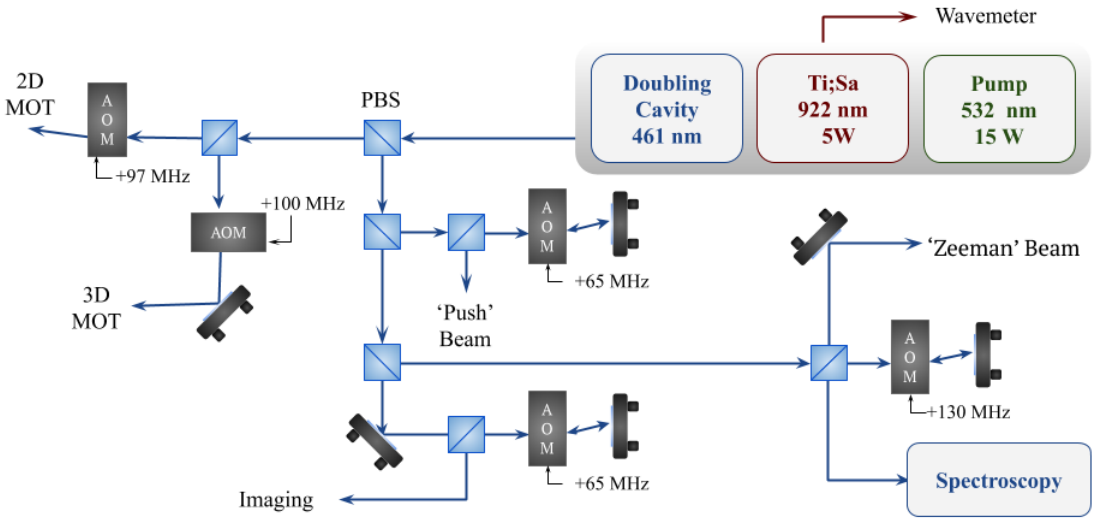

Figure 11 – Optical setup of the blue laser system. It provides light beams at the right frequency for each stage of the experiment, that is, the 2D and 3D-MOT, spectroscopy to lock the MSquared laser, imaging beam for atom number measurement, the "Zeeman beams" and the push beam. AOM: Acousto-optic modulator. PBS: polarizing beam spliter; AOM: acousto-optic modulator.

3.4 Blue MOT Characterization

3.4.1 Loading rate

The equilibrium of the number of atoms trapped in the MOT is reached when the loading rate R of atoms balances the loss rate τ. The number of atoms in a MOT evolves as

$$N(t) = R\tau(1 - e^{-t/\tau}). \tag{3.3}$$

The rate R depends on the capture ability of MOT, determined by experimental parameters such as size and intensity of the trapping laser beams and the magnetic field gradient. The loss rate τ is due to collisions of the trapped atoms with the atoms from residual background gas, which are at room temperature. It also can be atributed to events of inelastic collisions between the trapped atoms, where they acquire enough velocity to escape from the trapping potential (28).

In the blue MOT, we currently trap $N \sim 1 \times 10^6$ atoms. Figure 12 shows the evolution of the atom number of the MOT as a function of time, beginning from the turning on of trapping beams. From the data it was performed a fitting using equation 3.3 which the obtained loading rate is $R = 1.4\ \mathrm{s}^{-1}$ and a loss rate of $\tau = 0.7$ s. It is necessary

approximately 3.5 s to reach the maximum stationary number of atoms.

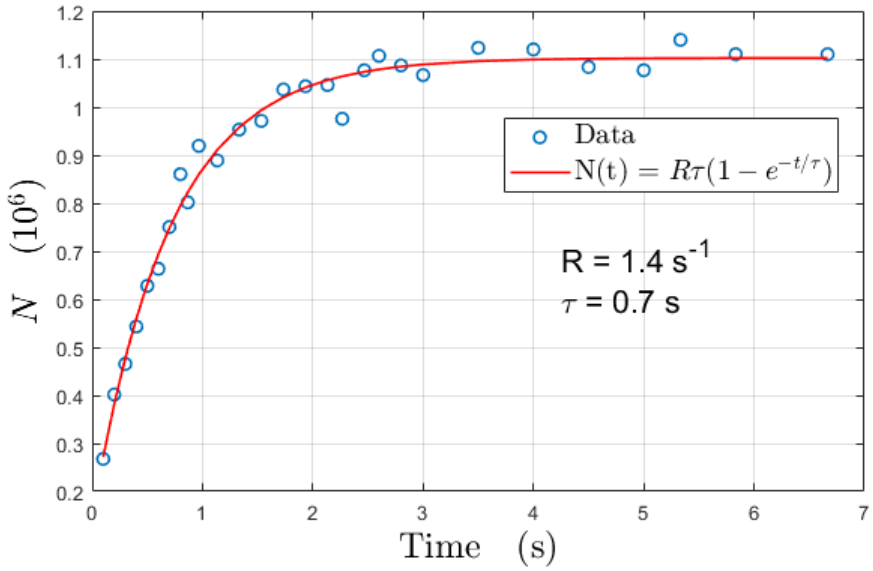

Figure 12 – Blue MOT loading rate.

3.4.2 MOT temperature

To measure the temperature of the atomic cloud we can measure its free expansion when the MOT is turned off. For a MOT, in the linear approximation, the trapping potential is approximately Gaussian, hence the spatial distribution will be also approximately Gaussian. In this linear approximation the MOT beams are described as plane waves with infinite radial extend. Considering a Gaussian distribution for the atomic cloud at $t = 0$ with an initial radius of $\sigma_{i,0}$, in which $i = x,\ y,\ z$. After some time t, each atom with initial velocity $\mathbf{v}$ will have traveled from its initial position $\mathbf{r_0}$ by an amount $\mathbf{v}t$. The probability to find an atom in a volume dr^3 is given by

$$f(\mathbf{r}, \mathbf{v}, t > 0) \propto \prod_{i=x,y,z} e^{-(r_i - v_i t)^2 / 2\sigma_{i,o}^2}. \tag{3.4}$$

It is necessary that equation 3.4 respect the Maxwell-Boltzmann distribution $g(v_i, T)$, which gives the probability that a non-interacting atom at temperature T has a certain velocity along a specific direction i. The spatial distribution at a later time is obtained by integrating over all the possible velocities

$$f(\mathbf{r}, t) \propto \prod_{i=x,y,z} \int_{-\infty}^{+\infty} e^{(-r_i - v_i t)^2 / 2\sigma_{i,o}^2)} g(v_i, T_i) dv_i. \tag{3.5}$$

By the equipartion theorem, we have

$$g(v,T) = \left[\frac{m}{2\pi k_B T}\right]^{1/2} e^{-mv^2/2k_BT} \tag{3.6}$$

To consider the impact of gravity, we just need to replace $r_z \to r_z + gt^2/2$ into equation 3.5. Now, inserting equation 3.6 into 3.5 and integrating over v_x, v_y and v_z

$$f(\mathbf{r},t) \propto e^{-x^2/2\sigma_x(t)^2} e^{-y^2/2\sigma_y(t)^2} e^{-(z+gt^2)^2/2\sigma_z(t)^2}, \tag{3.7}$$

where

$$\sigma_i^2(t) = \sigma_{i,0}^2 + \frac{k_B T_i}{m} t^2. \tag{3.8}$$

With equation 3.8 we can extract the temperature of the atomic cloud measuring its free expansion for different times of flight using the absorption imaging technique (29).

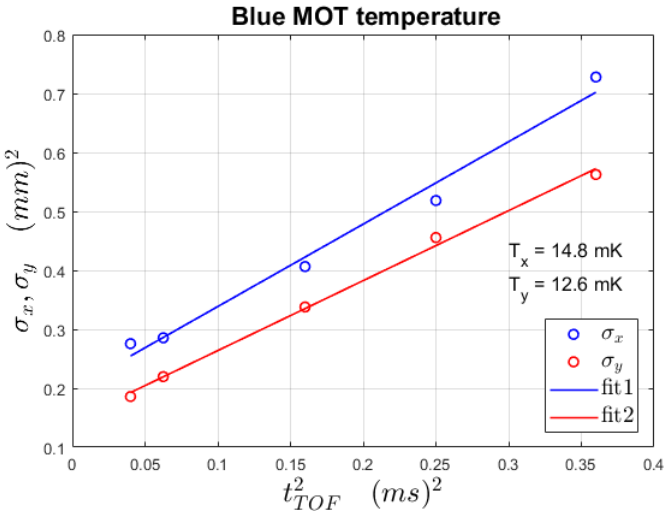

Figure 13 – Temperature measurement of the 3D blue MOT using absorption imaging.

Figure 13 shows a measurement of $\sigma_{x,y}$ of the atomic cloud for several times of flight. From a linear fit made using equation 3.8 we could obtain the temperature of the cloud for the x and y-direction. The temperature difference between the x and y-axis is attributed to its initial asymmetric shape. The mean temperature is $\sim$ 13.7 mK.

3.5 Narrow-line cooling

Cooling the strontium atoms using the intercombination line is one of the goals of the experiment. Unfortunately, we have not reached it yet. Nevertheless, a theoretical discussion will be presented in the following.

Lower temperatures can be reached making use of narrow line transitions where $\Gamma/\omega_r \sim 1$, or less. For ^{88}Sr $^1S_0 - ^3P_1$ transition, which has linewidth of $\Gamma = 2\pi \times 7.6$ kHz, this ratio is $\Gamma/\omega_r \sim 1.5$. In this regime, the relevant energy scale depends on the saturation parameter s. This process depends on the laser detuning $\Delta = \omega_L - \omega_0$, where ω_L is the laser frequency and ω_0 the atomic resonance frequency. For the transition of interest and $\Delta < 0$,the MOT dynamics can be divided into three regimes that will be discussed in the following for a qualitative understanding of the effects of Δ and s (30).

3.5.1 Regime (I)

It is defined for $s \gg 1$ and $\Delta < \Gamma'$, where $\Gamma' = \Gamma\sqrt{1+s}$ is the power-broadened linewidth. This regime is similar to standard Doppler cooling, where the radiative force produces a damped harmonic motion. Consequently, the trapping potential is approximately harmonic.

For the strontium intercombination line, the ratio between the radiation pressure and the gravitational force is $F_{rp}/F_g \sim 10$. For this reason, it is necessary to take into account the gravitational force to the MOT force in the vertical direction. For a slowly moving atom near the origin, we have

$$F_{1DMOT} = mg + \alpha v + \frac{\alpha\beta}{k} z \tag{3.9}$$

where

$$\alpha = \frac{k}{\Gamma} \frac{8\hbar k s \Delta}{(1 + s + 4\Delta^2/\Gamma^2)^2}, \tag{3.10}$$

$$\beta = \mu \partial B_z. \tag{3.11}$$

The force acts as a damped harmonic oscillator since $\Delta < 0$ implies $\alpha < 0$, where α is the damping coefficient and $\alpha\beta/k$ the spring constant.

3.5.2 Regime (II)

In this case, we consider $s \gg 1$ and $|\Delta| > \Gamma'$. The trapping potential adopts a box-like geometry and the atomic motion describes a balistic flight between the wall

boundaries. The viscous damping and gravity eventually cause the atoms to settle down to the minimum potential in the z-axis, which is tilted by gravity. Since the Zeeman shift is different for σ^+ and σ^- light, the downward propagating MOT beams will be seen by the atoms as shifted out of resonance, making them interacting primarily with the upward propagating MOT beams. The equilibrium position z_0 occurs when the radiation force of this beam balances the gravitational force, leading to (31)

$$F_{upwards} = F_{rp} + F_g \tag{3.12}$$

$$F_{upwards} = \alpha v + \frac{\alpha\beta}{k}(z - z_0) \tag{3.13}$$

where

$$\alpha = -\frac{4g^2m^2}{\Gamma^2\hbar s}\sqrt{-4\left(1 + s + \frac{\Gamma\hbar ks}{2gm}\right)} \tag{3.14}$$

with β the same as before and z_0 is the equilibrium position given by

$$z_0 = \frac{\Delta}{\beta} + \frac{\Gamma}{2\beta}\sqrt{-\frac{\Gamma\hbar ks}{2mg} - s - 1}. \tag{3.15}$$

With $\Delta < 0$ and $k > 0$ (propagating beam towards positive z). The force acts the same way as describe earlier, but now with a position-dependent term. The potential energy minima are determined by the equilibrium position z_0, which depends on the detuning. As Δ increases, z_0 shifts vertically, an effect that clearly shown in Fig. 14(c).

3.5.3 Regime (III)

In this case we considere $s \sim 1$, where the single photon recoil governs the trap dynamics requiring a quantum treatment of the atomic motion. This regime will not be discussed here, since we do not intend to reach it in the experiment.

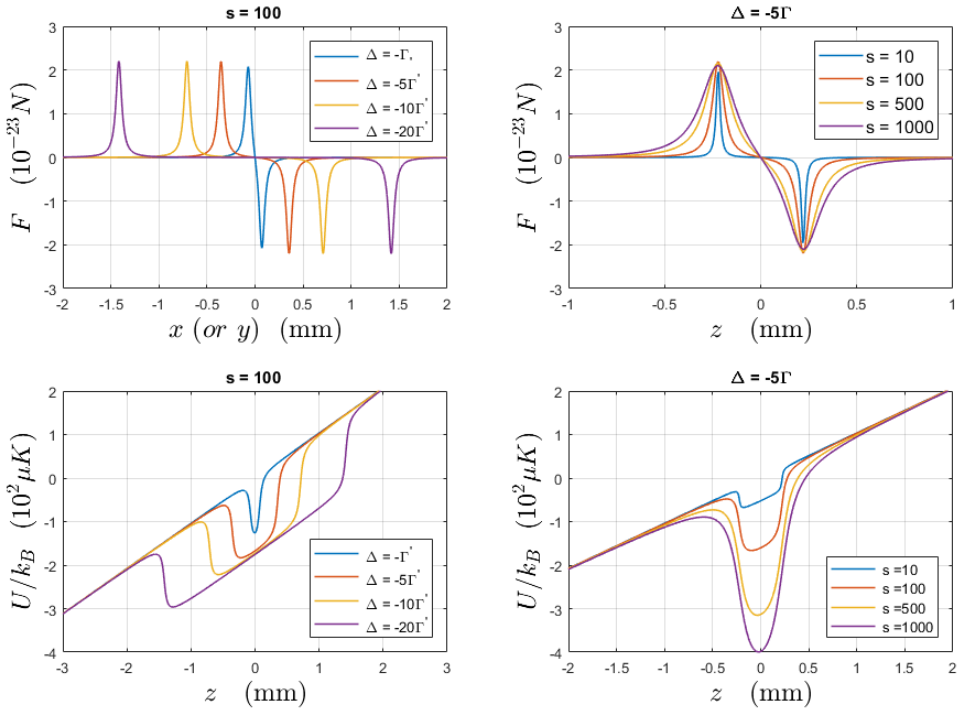

Figure 14 – (a, b) Semiclassical radiative force versus position for different detunings and saturation parameters, respectively.(c, d) The potential energy in the z-direction for different detunings and saturation parameters, respectively.

4 Frequency and phase stabilization of diode lasers

Nowadays we can find a considerable variety of diode lasers for wide range of frequencies, from visible ligtht to UV and IR. Most of them are relative cheap, since they are produced in large scale, and compact, making them a powerful tool for several research areas, from atomic physics to medicine (32, 33).

On the other hand, diode lasers present some issues such as large linewidth and fluctuations in the emitted wavelength. Fortunately, several lock techniques have been developed and can be applied to overcome these problems.

In our experiment, the diode lasers operating near the 689 nm intercombination line fulfill three tasks: (1) cool the atoms until a temperature close to the recoil temperature; (2) generate the vertical standing wave along the ring cavity axis to capture the Sr atoms and let them perform Bloch oscillations under the action of gravity; (3) inject a probe light in the ring cavity to measure the motional state of the matter-wave.

The low temperature will be achieved through MOT operated on the strontium ${}^1S_0 - {}^3P_1$ transition. Since this transition has a linewidth of 7.6 kHz, the laser responsible for the cooling process must have a linewidth narrower than the transition and also a high output power. To accomplish this, first, a laser (subsequently called master laser) can be locked to a high finesse cavity through the Pound-Drever-Hall technique. After that, a second laser can be locked to the first by injection locking.

A third laser is used for generating an optical lattice. Because the employed atomic line is narrow, we need to tune the laser sufficiently close to resonance in order to have a noticeable interaction between atoms and the optical lattice, i.e., for the optical lattice to be deep enough. This bears the advantage the laser is within a frequency range, where common optical phase-locking techniques are available. In this chapter, the aforementioned techniques, which are necessary for laser frequency stabilization, will be discussed.

4.1 Reference cavity

A reference cavity is an optical resonator which is used as an optical frequency standard. The optical frequency of a single-frequency laser can be stabilized to the frequency of a resonance of the reference cavity, effectively transferring the higher frequency stability of the cavity to the laser. Such stabilization of frequency locking can be achieved with an electronic feedback system such as the Pound–Drever–Hall method, which will be described

in section 4.2.

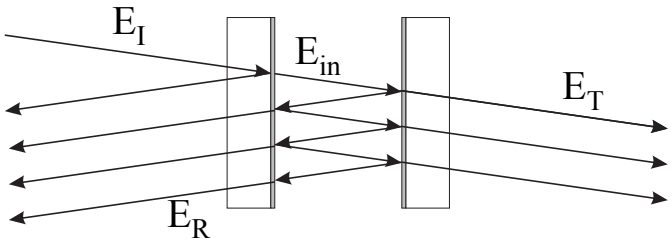

Figure 15 – Representation of the electric field in a Fabry-Perot cavity, where E_I is the incident field, E_R is the reflected one, E_{in} is the intracavity electric field and E_T is the transmitted field.

To describe how it works, we are going to consider the properties of the Fabry-Perot cavity. We can write the incident electric field as

$$E_I = E_0 e^{i\omega t} \tag{4.1}$$

The reflected light consists of the beam that is promptly reflected off the mirror plus the beam that leaks from the standing wave that forms inside the cavity (see Figure 15) . Therefore, the reflected beam has multiple phase components due to the different traveling paths inside the cavity for each transmitted beam. For a cavity with symmetric mirrors of reflectivity r and transmitivity $t = \sqrt{1 - r^2}$, the total reflected electric field amplitude can be written as (34)

$$E_R^{tot} = -rE_I + E_I \sum_{m=1}^{\infty} t^2 r^{2m-1} e^{im2\Delta\phi}, \tag{4.2}$$

which consists of the superposition of the electric field amplitudes of light that was promptly reflected and the leakage beam with different m round-trips inside the cavity. The factor $\Delta\phi$ consists of the phase accumulated due to the trip from one mirror to another. The relation between E_I and E_R can be given in terms of the cavity reflection coefficient $F(\omega)$ as

$$F(\omega) = \frac{E_R^{tot}}{E_I} = \frac{r\left(e^{2i\Delta\phi} - 1\right)}{1 - r^2 e^{2i\Delta\phi}}. \tag{4.3}$$

The total reflection intensity is given by the Airy formula (35)

$$I_R^{tot} = I_0 \frac{4r^2 \sin^2(\Delta\phi)}{t^4 + 4r^2 \sin^2(\Delta\phi)} = I_0 \frac{\sin^2(\Delta/\delta_{fsr})}{(2\mathcal{F}/\pi)^2 + \sin^2(\Delta/\delta_{fsr})}, \tag{4.4}$$

where the phase factor $\Delta\phi$ is given by in terms of the frequency detuning Δ between the light field and the cavity, and also by the free spectral range δ_{fsr}, which is the spacing

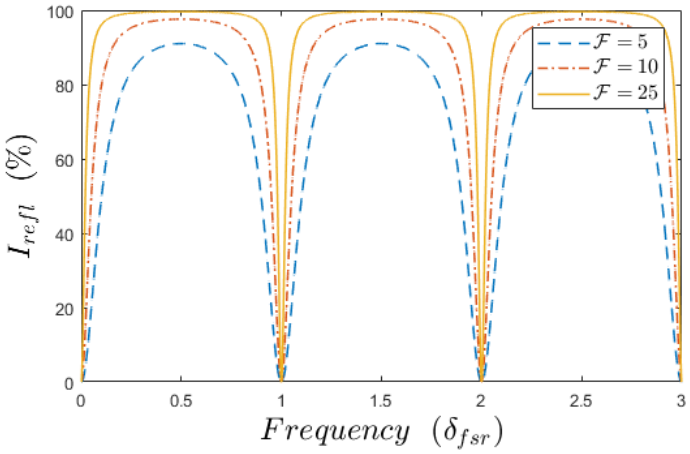

Figure 16 – Reflected intensity from a cavity for different finesses $\mathcal{F}$ for a mirror spacing of $d = 10\ cm$.

in frequency (wavelength) between two successive minimum of the reflected intensity or maximum of the transmitted intensity ($\Delta\phi = 2\pi L/\lambda = \omega L/c = \omega/2\delta_{fsr}$). The free spectral range is given by

$$\delta_{fsr} = \frac{c}{2L}, \tag{4.5}$$

where L is the distance between the two mirrors of the cavity. The total reflected intensity can also be expressed in terms of the cavity *finesse* $\mathcal{F}$ that describes often how much a photon can travel inside the cavity before being absorbed or transmitted by the mirrors. It is given by the cavity characteristics such as the mirror reflectivity $R = |r|^2$ or by the cavity linewidth κ (full width at half maximum of the transmitted or reflected intensity)

$$\mathcal{F} = \frac{\pi\sqrt{R}}{1-R} = \frac{2\pi\delta_{fsr}}{\kappa}. \tag{4.6}$$

We can observe in Figure 16 that by increasing $\mathcal{F}$ the spectral width of the cavity gets sharper. It is valid to note that the cavity finesse is only described by the quality of the mirror while the free spectral range changes with the spacing between the mirrors. Therefore, the resonance frequencies are stable when the cavity length is stable. If a high-finesse cavity is well isolated from the environment to avoid mechanical and thermal variations in the mirrors, it can be used as a frequency reference for laser frequency stabilization.

4.2 Pound-Drever-Hall locking

As described in the previous section, we can use a stable Fabry-Perot cavity as a frequency reference for laser stabilization. To accomplish this, we could think of monitoring the light reflected from the cavity and use a servo loop to adjust the laser frequency to stay always in the resonance with the cavity, holding the reflected intensity at zero. Unfortunately, this method suffers from a few flaws. It is not possible to distinguish intensity fluctuations of the laser from its frequency instability. Also, when a departure from the total transmission condition happens, one would not be able to determine to which side of the resonance the laser has drifted.

The Pound-Drever-Hall (PDH) method overcomes these flaws. The error signal represents a dispersive lineshape as a function of the frequency. This provides a signal that is antisymmetric across the resonance, so that indicates to which side of the resonance the laser has drifted. This technique decouples the frequency measurement from the intensity of the laser, and it is not limited by the response time of a Fabry–Perot cavity (34).

The reflected intensity is always positive and its derivative tells us each side of the resonance we are on. Above resonance, the derivative is positive and the intensity will respond in phase with frequency variations. Below resonance, the derivative is negative and the reflected intensity will vary 180° out of phase from the frequency. Exactly on resonance, the reflected intensity is at a minimum and a small frequency variation will produce a change in the reflected intensity. We can obtain a signal which is proportional to the derivative with the PDH technique, which will be explained next.

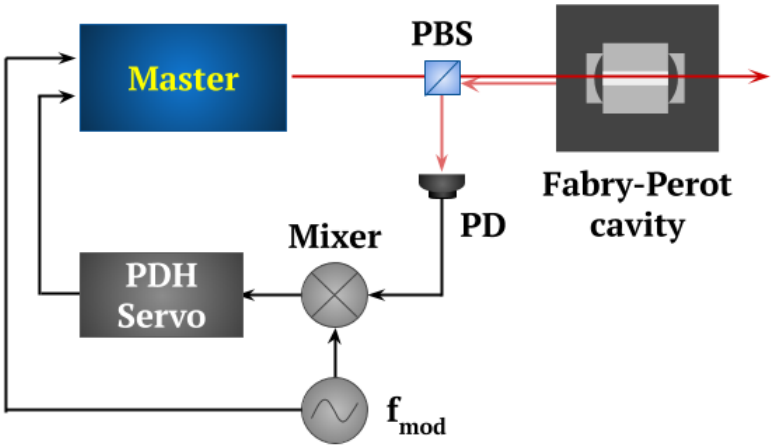

Figure 17 – Basic setup for PDH locking. The f_{mod} is responsible to produce the side bands modulation. PD is a photodetector and PBS a polarizing beam splitter.

4.2.1 PDH error signal

The PDH technique is based on the generation of an error signal that depends on the phase of the reflected electric field from the cavity. This is achieved by phase-modulation of the incident light on the cavity. The carrier of frequency ω is modulated with an electronic signal of frequency Ω, generating sidebands separated by positive and negative multiples of Ω from the central frequency ω. Considering a monochromatic beam, the modulated electric field can be written as

$$E_I = E_0 e^{i(\omega t + \beta sin\Omega t)}, \tag{4.7}$$

where E_0 is the amplitude and β is the modulation index. Equation 4.7 the can be expanded into Bessel Functions as

$$E_I = E_0 e^{i\omega t} \sum_{n=-\infty}^{\infty} J_n(\beta) e^{in\Omega t}. \tag{4.8}$$

Considering $\beta \ll 1$, the first order sidebands are small compared to the carrier and the higher other sidebands can be neglected. Then, we can rewrite the equation above as (34)

$$E_I \approx E_0 \left[J_0(\beta) e^{i\omega t} + J_1(\beta) e^{i(\omega+\Omega)t} - J_1(\beta) e^{i(\omega-\Omega)t} \right]. \tag{4.9}$$

The incindent field now is a superposition of the carrier beam of frequency ω and the two sidebands at $\omega \pm \Omega$. From equation 4.3 we can write the total reflected electric field from the cavity as three independent beams multiplied by its corresponding reflection coefficient

$$E_R^{tot} = E_0 \left[F(\omega) J_0(\beta) e^{i\omega t} + F(\omega+\Omega) J_1(\beta) e^{i(\omega+\Omega)t} - F(\omega-\Omega) J_1(\beta) e^{i(\omega-\Omega)t} \right]. \tag{4.10}$$

However, what we measure is the intensity of the beam that is given by the relation $P_r = |E_R|^2$. We can calculate the power P_c due to the contribution of the carrier beam and the power P_s of the first order sidebands as

$$\begin{aligned} P_c &= |E_I|^2 J_0^2(\beta) \\ P_s &= |E_I|^2 J_1^2(\beta) \end{aligned} \tag{4.11}$$

The total reflected power is given by

$$
\begin{aligned}
P_{r,t} = P_c|F(\omega)|^2 + P_s\left(|F(\omega+\Omega)|^2 + |F(\omega-\Omega)|^2\right) \\
+ 2\sqrt{P_c P_s}\,\mathrm{Re}\left[F(\omega)F^*(\omega+\Omega) + F^*(\omega)F(\omega-\Omega)\right]\cos\Omega t \\
+ 2\sqrt{P_c P_s}\,\mathrm{Im}\left[F(\omega)F^*(\omega+\Omega) + F^*(\omega)F(\omega-\Omega)\right]\sin\Omega t \\
+ \left(O[2\Omega]\right), \quad (4.12)
\end{aligned}
$$

the signal consists of terms oscillating with Ω from the interference between the carrier beam and the sidebands, and terms of frequency 2Ω from the interference between the sidebands. When the carrier is near resonance and the modulation frequency is high enough ($\Omega \gg \delta_{fsr}/\mathcal{F}$), we can assume that the sidebands are totally reflected, $F(\omega \pm \Omega) \approx -1$. In this regime, we have

$$
F(\omega)F^*(\omega+\Omega) - F^*(\omega)F(\omega-\Omega) \approx -i2\,\mathrm{Im}\{F(\omega)\}, \quad (4.13)
$$

that is a purely imaginary term. The contribution of $\cos(\Omega t)$ in equation 4.12 can be neglected and we can use the term that varies with $\sin(\Omega t)$ to generate an error signal. Therefore, we can isolate this component using a mixer that is, we can multiply the $P_{inc} \propto \sin(\Omega t)$ from the photodetector with $\sin(\Omega t)$ from an oscillator. The result is a DC component and a $\cos(2\Omega t)$ term. Using a low pass filter, we can isolate the DC component and the result is the Pound-Drever-Hall error signal

$$
P_\epsilon = 2\sqrt{P_c P_s}\,\mathrm{Im}\left[F(\omega)F^*(\omega+\Omega) - F^*(\omega)F(\omega-\Omega)\right] \quad (4.14)
$$

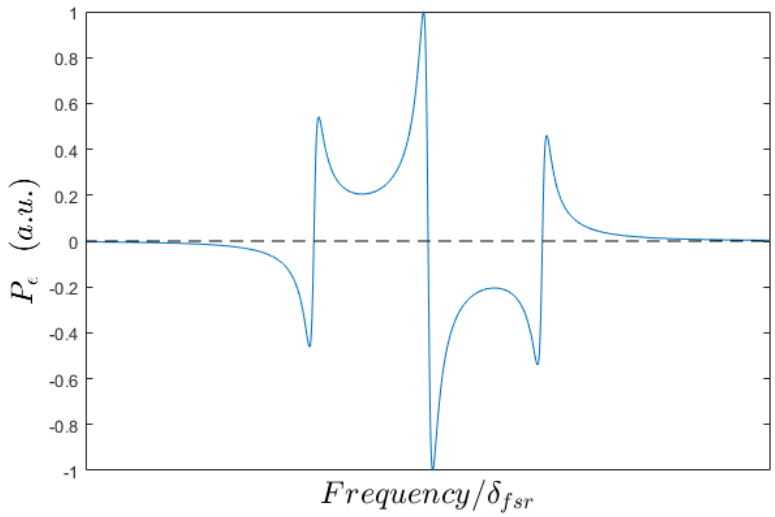

Figure 18 – The Pound-Drever-Hall for high modulation frequency

Figure 18 shows the PDH error signal against laser frequency. It presents a slope with a zero crossing centered at the cavity resonance and two side fringes. As expected, the signal is antisymmetric, and there is a large frequency band over which its sign indicates which side of the cavity resonance the laser is tuned. Additionally, the error signal has a steep slope near resonance representing a large sensibility for deviations from resonance, which is helpful for the servo loop.

Near resonance the reflected power vanishes, since $|F(\omega)|^2 \approx 0$. To approximate the error signal in this regime, we can recover the terms to first order in $F(\omega)$

$$P_r \approx 2P_s - 4\sqrt{P_c P_s}\,\mathrm{Im}\{F(\omega)\}\sin\Omega t + (O[2\Omega]). \tag{4.15}$$

Near resonance, we have

$$\frac{\omega}{\delta_{fsr}} = 2\pi N + \frac{\Delta\omega}{\delta_{fsr}}, \tag{4.16}$$

where N is and integer and $\Delta\omega$ is the detuning of the laser from the resonance. Now, considering a high finesse cavity, the reflection coefficient becomes (34)

$$F(\omega) \approx \frac{i}{\pi}\frac{\Delta\omega}{\kappa}, \tag{4.17}$$

where κ is the cavity's linewidth. The error signal is given by

$$P_\epsilon \approx -\frac{4}{\pi}\sqrt{P_c P_s}\frac{\Delta\omega}{\kappa}. \tag{4.18}$$

The approximation is valid as long as $\Delta\omega \ll \kappa$. Writing the error signal in terms of real frequencies $f = \omega/2\pi$, and defining the proportionality constante D as

$$D \equiv -8\frac{\sqrt{P_c P_s}}{\kappa}, \tag{4.19}$$

the error signal then becomes $P_\epsilon = D\delta f$. As showed in Figure 18, the error signal is linear near resonance and presents a steep slope with a zero crossing, making an ideal condition for a servo loop to operate.

4.3 Laser injection locking

The injection locking technique is a way to stabilize the frequency of a diode laser, when one has another stable laser source available. It consists in forcing a laser to operate in a certain frequency regime by injecting light from a stable laser reference. This method is commonly used for high power laser sources that usually have a considerable intensity

but exhibit large phase noise and/or multimode frequency behavior in the frequency range of interest.

We are going to consider a high-power laser called slave laser and a master laser, which is the frequency reference. If the frequency of both lasers is close enough, by injecting light from the master laser into the resonator of the slave laser, it starts to operate exactly on the injected frequency. The higher injected power, the larger is the allowable frequency offset between the seed laser and the slave laser's resonance.

4.3.1 Principle of operation

The description presented here follows the derivations made by *Liu et al.* (36) that uses semiclassical laser rate equations. To describe it, we are going to consider the setup presented in Figure 19, where the master and the free-running slave laser field are given by respectively

$$\begin{aligned} E_m &= A_m e^{-i\omega_m t} e^{i\phi_m(t)}, \\ E_s &= A_s e^{-i\omega_s t} e^{i\phi_s(t)}. \end{aligned} \tag{4.20}$$

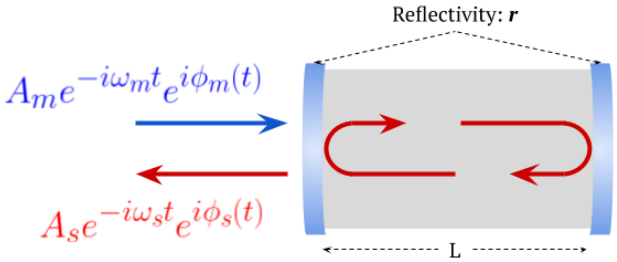

Figure 19 – Schematic representation of injection field into a slave laser.

The phase difference between the both fields is denoted by $\phi(t) = \phi_s(t) - \phi_m(t)$. Now, considering the semiclassical laser rate equations we can describe the impact of the master laser field in the slave laser

$$\frac{dA(t)}{dt} = \frac{1}{2} g \left[N(t) - N_{th}\right] A(t) + \kappa A_m cos\phi(t), \tag{4.21}$$

$$\frac{d\phi(t)}{dt} = \frac{\alpha}{2} g \left[N(t) - N_{th}\right] - \kappa \frac{A_m}{A(t)} sin\phi(t) - \Delta\omega, \tag{4.22}$$

$$\frac{dN(t)}{dt} = J - \gamma_N N(t) - \left[\gamma_p + g(N(t) - N_{th})\right] A(t)^2, \tag{4.23}$$

where $A(t)$ is the field amplitude normalized as $A^2(t) = S(t)$, and $S(t)$ is the photon number. $N(t)$ is the number of carriers in the slave laser, and the other parameters are described in Table 1.

Parameter	Description
g	laser gain coefficient
N_{th}	threshold carrier number
κ	coupling coefficient
α	linewidth enhancement factor
γ_p	photon decay rate
γ_N	carrier recombination rate
J	pump current normalized by electron charge
$\Delta\omega$	frequency difference between the master and the free running slave $\omega_m - \omega_s$

Table 1 – Injection locking laser parameters.

The parameter κ describes the rate at which the photons of the master laser enter into the slave laser cavity and is given in terms of the cavity quality factor

$$\kappa = \frac{\omega_s}{2\mathcal{Q}}. \tag{4.24}$$

In the steady state in which the slave laser carrier frequency tracks that of the master laser, it provides a frequency locking range whitin certain bounds. It can be be obtained through the stady state solution os equations 4.21-4.23, which gives (37)

$$-\kappa\sqrt{1+\alpha^2}\sqrt{\frac{P_{inj}}{P_s}} < \Delta\omega < \kappa\sqrt{\frac{P_{inj}}{P_s}}, \tag{4.25}$$

in which P_{inj} is the master laser fraction power used for the injection locking, P_s is the power of slave laser and α describes the amplitude phase coupling (i.e., phase change due to the change of carrier density dependent refractive index). From equation 4.25 we can see that the locking range is determined by the amplitude ratio between the fields and by the cavity quality factor since $\kappa \propto \mathcal{Q}^{-1}$. Therefore, lasers with low $\mathcal{Q}$ are easier to lock. On the other hand, this leads to increased laser linewidth that reduces the phase noise performance of the injection locking systems. For higher injection ratio P_{inj}/P_s also results in a large locking range, which makes the lock easier to achieve.

It is necessary that equation 4.22 has a steady-state solution to be possible to obtain a stable optical injection. Physically, it means the slave laser must reduce its gain, or the carrier number, to achieve a steady-state ($\omega_s = \omega_{inj}, \phi$ is a constant value) that locks to the master laser. Due to the nonzero factor α, the cavity mode is red-shifted which causes the asymmetry of the locking range (36).

4.4 Optical phase-locked loop

An optical phase-locked loop (OPLL) can be realized with a monomode slave laser that is phase-compared with a master laser. The phase detector system generates an output signal that is proportional to the phase difference between the two lasers. This signal is then fed to the slave laser and used to control its frequency. In a heterodyne OPLL, the phase difference of two lasers with different wavelengths is locked to a local oscillator, which is a stable reference phase.

4.4.1 Basic description

Let's consider a slave laser that needs to be offset locked to a master laser. Figure 20 shows a schematic OPLL feedback system that enables electronic control of the slave laser. It consists of mixing the light of both lasers in a photodetector PD. The PD generates a current proportional to the measured signal, which is amplified and mixed down with a radio frequency (RF) signal. The resulted signal is then filtered and fed back to the laser to be stabilized.

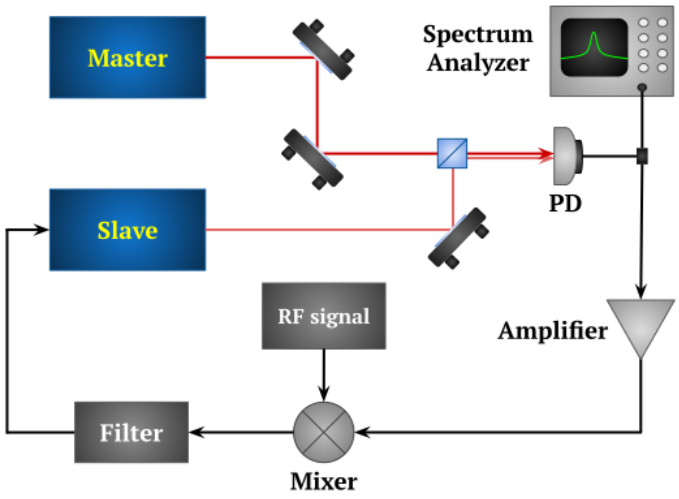

Figure 20 – Schematic setup for phase-locked loop. PD: photodetector.

The electric field of the slave E_s and the master E_m that arrives in the photodetector can be written as

$$\begin{aligned} E_s &= A_s \cos(\omega_s t + \phi_s(t)) \\ E_m &= A_m \cos(\omega_m t + \phi_m(t)). \end{aligned} \tag{4.26}$$

Considering that the PD has a responsivity ρ, the current generated by the detected

signal is given by (38)

$$i_{PD}(t) = \rho(A_m^2 + A_s^2 + 2A_m A_s \cos\left[(\omega_m - \omega_s)t + (\phi_m(t) + \phi_s(t))\right]). \tag{4.27}$$

The equation above shows that the PD act as a frequency mixer. We can define the photodetector gain as function of the average input signals amplitude $K_{PD} = 2\rho\langle A_s A_m\rangle$. The current produced by the PD is then mixed in a mixer with an RF signal of $A_{RF}\sin(\omega_{RF} + \phi_{RF}t)$, in which the mixer has gain K_{mix}. The resulting output signal is given by (39)

$$i_{mix}(t) = \pm K_{mix} K_{PD} A_{RF} \sin\left[(\omega_m - \omega_s \pm \omega_{RF})t + (\phi_m(t) - \phi_s(t) \pm \phi_{RF}(t))\right]. \tag{4.28}$$

The current is then amplified with a gain K_a, filtered by a low-pass filter that only lets pass the lowest of both frequencies $\omega_m - \omega_s \pm \omega_{RF}$, and fed into the slave laser. The frequency shift in the slave laser is proportional to the input current with a gain of K_s

$$\delta\omega_s = -K_s K_a i_{mix}(t). \tag{4.29}$$

The frequency of the slave laser decreases when the current increases. We can denote the total gain due to the various components of the loop as $K = K_s K_a K_{mix} K_{PD}$. When the slave laser is locked by an active electronic feedback loop, the locking system creates a frequency shift given by

$$\delta\omega_s = -K \sin\left[(\omega_m - \omega_s \pm \omega_{RF})t + (\phi_m(t) - \phi_s(t) \pm \phi_{RF}(t))\right]. \tag{4.30}$$

Equation 4.30 has the characteristics of an error signal, as was described before: it is antisymmetric with respect to the locking point. Ideally, frequency and phase are locked, in which the phase is locked modulus 2π. The error signal is used to apply an electronic feedback to the slave laser and correct it, in order to keep the frequency locked with an offset, satisfying the condition below

$$\Delta\omega_{fr} = \omega_m - \omega_s + \omega_{RF}, \tag{4.31}$$

that determines the difference between the frequency of the free-running slave offset by the RF frequency and the master laser. When the laser is locked, in steady-state its frequency and phase will not be changed in time

$$\begin{aligned} \omega_s &= \omega_m + \omega_{RF} \\ \phi_s &= \phi_m + \phi_{RF} + \phi_e. \end{aligned} \tag{4.32}$$

The parameter ϕ_e is the steady-state phase error due to the feedback current maintaining the lock. It is given by (39)

$$\phi_e = \sin^{-1}\left(\frac{\Delta\omega_{fr}}{K}\right). \tag{4.33}$$

From this relation, we can see that if the total DC gain K is large enough, it minimizes the phase fluctuations. For $\phi_e \sim 0$, the phase of the locked slave laser is exactly the phase of the master shifted by the RF frequency. Then, the optical phase can be adjusted simply by controlling the RF frequency.

4.5 Which locking system to choose?

In our experiment, where various lasers are used, each presented locking method serves different purposes described in the following.

- **Lock to a stable cavity:** Provides an absolute frequency reference if the cavity is stable and if there is no other reference. In the laboratory, the entire laser system is referenced to an ultra-stable cavity. Note that there is an atomic reference: the strontium 689 nm intercombination line. However, while atomic transitions have extremely good reproducibilities and long-term stabilities, they do not provide good signal-to-noise ratios and short-term stabilities for locking purposes.
- **Injection locking:** It serves to obtain a large power at a certain frequency, from a high power but multimode diode, for which the OPLL is not possible.
- **Optical phase-locked loop:** Very stable lock system, locks two lasers in phase, which is useful for example for coherent manipulation of atomic states in two different transitions at the same time; or to maintain lasers with a fixed frequency difference; also to lock the frequency of a second laser, if you have a first one already locked to another reference. However, it only works for two lasers that are already singlemode when they are free running.

5 Experimental setup and characterization

As mentioned in the previous chapter, the diode lasers operating near the 689 nm intercombination line fulfill three tasks: (1) cool the atoms until a temperature close to the recoil temperature; (2) generate the vertical standing wave along the ring cavity axis to capture the Sr atoms and let them perform Bloch oscillations under the action of gravity; (3) probe the atomic state in the ring cavity measuring the motional state of the matter-wave. Theses tasks were achieved through the laser locking technique discussed in the previous chapter. Figure 21 shows the block diagram of the laser lock scheme in which each setup and characterization will be discussed in the following.

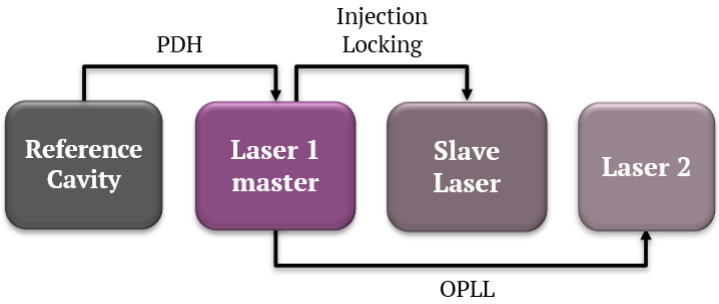

Figure 21 – Block diagram representing the locking scheme.

5.1 Pound-Drever-Hall setup

The first step to build the whole laser locking scheme is to have a reference laser that is called the master laser. Figure 22 shows the schematic setup for laser 1 (DLC pro, Toptica) which is our master laser. The laser 1 is coupled to the reference cavity (ATThinFilms) to a mode that is $\Delta = 495$ MHz far from the strontium $^1S_0 - ^3P_1$ transition ($\nu_{Sr} = 434.829121311$ THz). The signal reflected from the reference cavity is detected through the photodetector PD1 and sent to the Pound-Drever-Hall detector (PDH, Toptica), which is a built-in module that features an internal 20 MHz frequency modulation source for modulating the diode laser current via a bias-T directly at the laser diode. The PDH also demodulates the PD1 signal phase sensitively to produce a dispersive error signal. The error signal is then sent to the fast analog linewidth control (FALC, Toptica), a commercial PID locking module responsible to keep the laser locked to the cavity.

The light transmitted through the cavity is sent to the photodetector PD2, which in turn sends the signal to an oscilloscope. We use this signal to verify and optmize the lock of the laser to the reference cavity.

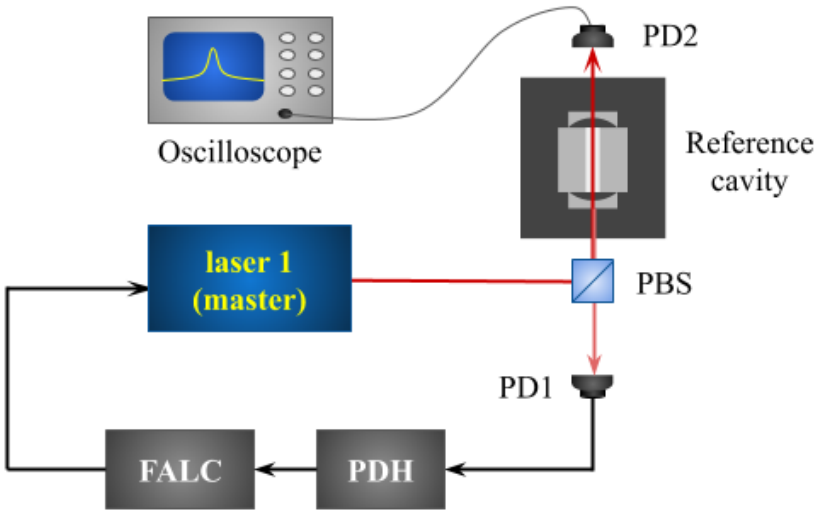

Figure 22 – Schematic setup used to lock the master laser to the reference cavity through PDH technique. The acronyms stand for: PBS: polarizing beam splitter; PD: photdetector; PDH: Pound-Drever-Hall stabilization (Toptica, PDH); FALC: fast analog linewidth control (Toptica, FALC).

5.1.1 Master laser linewidth

A way to characterize the quality of the locking technique is by analyzing the laser linewidth, since free-running diode lasers have a linewidth of the order of MHz. The laser linewidth can be measured by recording a beat note between two independent lasers, where either the reference laser has significantly lower noise than the one under test, or both lasers have similar performance. The comparison of the two light signals is typically accomplished by combining them in a photodiode detector. Usually, if the two light frequencies are similar enough, their beat frequency is in the radio or microwave range and can be conveniently processed by a spectrum analyzer.

The linewidth of a beat note for two uncorrelated laser is larger than the linewidth of each laser separately. However, the beat linewidth can be smaller if the phase noise of both lasers is at least partially correlated.

To measure the linewidth of the laser 1 we recorded the beat signal between this laser and another laser from a different experiment that is also locked to a reference cavity through PDH method. The signal was processed by a spectrum analyzer with 10 Hz resolution bandwidth (BWR). The result is shown in Figure 23, where the parameter w of the fitted Gaussian function is the FWHM, and give us the linewidth of the measured signal.

The fit of a Gaussian line profile to the beat signal reveals a linewidth of $w = (1,13 \pm 0,01)$ kHz. Since the signal is the convolution of both laser linewidths, the measured value is determined by the broader one. Physically, the lineshape is not necessarily Gaussian.

In fact, for white frequency noise we would rather expect a Lorentzian (40). However, for determining the linewidth either profile is good enough.

Also, it is important to note that the real laser linewidth can be narrower than the measured one. This is likely due to the fact that a 3-meter polarization-maintaining optical fiber was used to collect light from the laser of the other experiment for characterization of the beat signal, which could have led to spectral broadening due to polarization effects (41), and Doppler-broadening induced by mechanical, acoustic or thermal noise to which the fiber is subject.

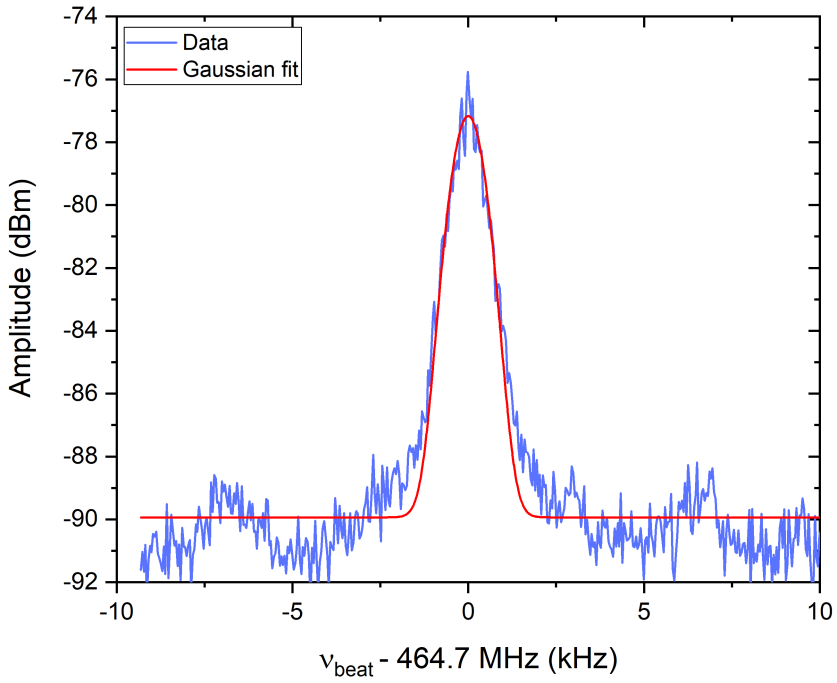

Figure 23 – Beat signal between two different lasers, each one locked to a reference cavity via the PDH technique.

5.2 Implementation of an injection locking

The injection locking does not require servo electronics for the laser to be stabilized, it is achieved basically by optical means. Firstly, it is necessary to provide a good mode matching between the seed beam of the master laser and the slave laser. This can be achieved easily with a telescope and a pair of anamorphic prisms.

Secondly, the master and the slave laser frequencies need to be close enough. For a frequency difference until the order of MHz, the power necessary for the seed beam is around μW. For differences of the order of GHz, it is necessary more power in the seed

beam (around mW), which can damage the slave laser diode. However, this also depends on the finesse of the slave laser cavity, as shown in section 4.3. If the finesse is artificially reduced by anti-reflection coating, much larger frequency differences are allowable with lower injection powers. Moreover, a Faraday isolator is required in the output of the slave laser, in order to avoid reflected light to reach the laser, which could disturb or damage it.

When all these requirements are fulfilled, the injection locking is achieved through an optimized optical alignment. It can be done by monitoring the frequencies of the slave and the master laser, or by observing to the spectrum of a Fabry-Perot cavity to which both, the slave and the master laser, are coupled. At the moment that the slave is injected, its frequency becomes the same as the seed beam, and its spectrum goes from multimode to single mode.

In our system, the injection locking is used to generate near-resonant light needed for the red MOT cooling stage. The laser 1, already stabilized to the reference cavity, is $\Delta = 495$ MHz far from the Sr line ($\nu_{Sr} = 434.829\ 121\ 311$ THz). To overcome the gap, the laser 1 is double-passed through the AOM1 (see Figure 24) where the light is frequency shifted by 400 MHz. Then, the shape of light beam is adjusted through a telescope and an anamorphic prism pair to match the slave laser beam shape. After that, the light is injected into the slave laser (HL6750MG, Opnext) via a Faraday isolator.

The light of the slave laser is coupled into a single-mode polarization-maintaining optical fiber. Upon exiting the fiber, the beam is expanded to a $1/e^2$ waist of 3.03 mm (not shown in Figure 24). The total power of 10 mW is divided into three equal intensity cooling beams. We use dichroic beam splitters to co-align the 689 nm and 461 nm MOT beams.

At the time of the transfer of the atoms from the blue to the red MOT, the atomic cloud has a temperature of around 5 mK, which corresponds to a Doppler broadening of 7 MHz at the frequency of the intercombination line. This is much larger than the linewidth of the 689 nm transition, which reduces the spectral overlap with the red MOT laser. To increase the efficiency of the cooling process, we modulate the frequency of the slave laser with the aid of the AOM1, whose frequency is modulated at 30 kHz and a modulation excursion, that starts at 8 MHz and is gradually reduced to 0 as the atomic cloud cools down (42), as shown in Figure 25.

5.2.1 Relative linewidth of the slave laser

The characterization of the injection locking is done as the same way as described in the previous section, but now making a beat signal between the laser 1 (master) and the slave laser. Figure 26(a) shows the beat signal between the master laser (locked to the super cavity through the PDH method) and the free-running slave laser. Since the slave

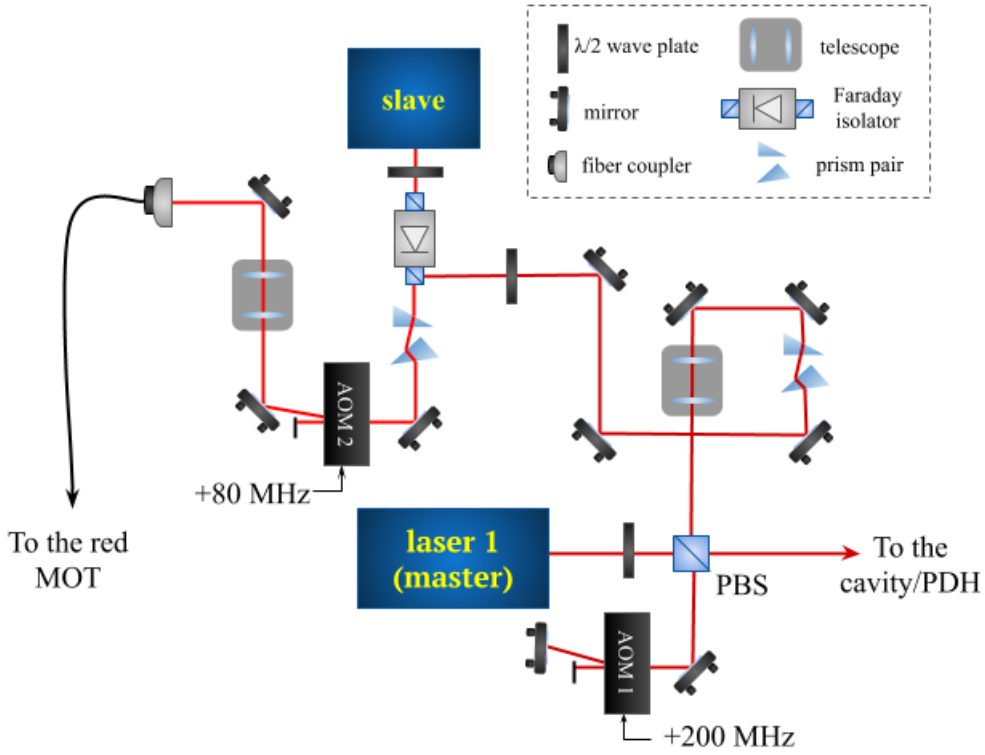

Figure 24 – Schematic representation of the injection locking setup.

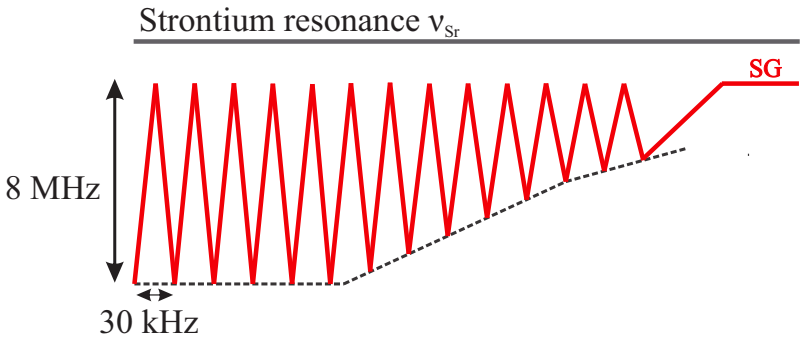

Figure 25 – Representation of the frequency modulation for the red MOT. SG: single frequency regime.

laser was not locked, its frequency fluctuates during the measurement. For this reason, the beat signal was averaged over 5 measurements with 1 MHz bandwidth resolution. A Gaussian fit was applied to the averaged line profile in which the obtained linewidth is $w = 8.8$ MHz. From the performed measurement presented in section 5.1.1, the master has a linewidth of the order of kHz. Hence, we can attribute the large linewidth only due to the slave laser, since it is compatible with the feature of a free-running diode laser.

Figure 26(b) shows the beat signal with 10 Hz of BWR when the injection locking is performed at the slave laser. The slave is correlated to the master with a beat note linewidth of $w = 18.6$ Hz, a value obtained through a Gaussian fit. Since the linewidth of

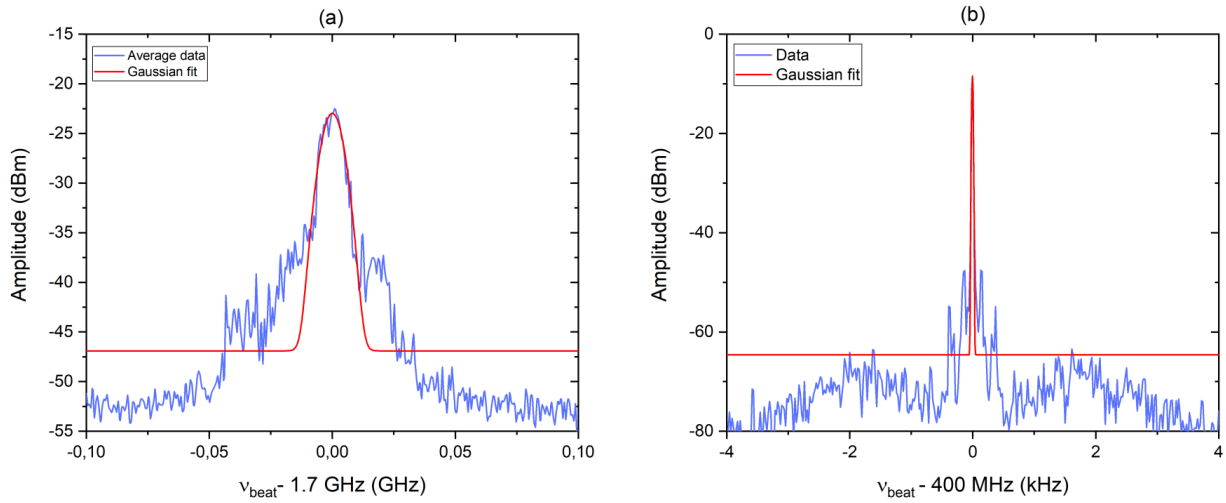

Figure 26 – Beat signal between the master (locked to the super cavity) and the slave laser for: (a) average over 5 measurements with 1 MHz of BWR for the free-running slave laser; (b) measurement with 10 Hz of BWR for the slave laser locked to the master through injection locking.

the master is of the order of kHz (showed in Figure 23) and thus much larger than 10 Hz, this means that the absolute linewidth of the slave is the same as the master. Once the slave laser is used to generate the cooling beams for the red MOT and the linewidth of the respective transition is 7.6 kHz, the laser linewidth has to be narrower than this. The performed measurements confirm that this requirement was fulfilled.

5.3 Phase-lock loop setup

After cooling the atoms using the narrow strontium transition ($^1S_0 - ^3P_1$) they will be subjected to a one-dimensional optical lattice, where they shall perform Bloch oscillations. Since the intercombination line has a linewidth of the order of kHz, it is sufficient to lock the laser to the mode of a ring cavity that is far from this atomic resonance. This is sufficient to produce the required dipolar forces while heating is avoided.

Our setup for phase-locking is based on the one proposed by *J. Appel et al.* (43), which is a robust design that is insensitive to fluctuations of the beat signal amplitude over a wide range and avoids the frequency range limitations of passive microwave mixers. The beat frequency is divided down digitally and inexpensive low-frequency references can be used. The schematic setup is shown in Figure 27, where the beat signal between the master laser and the laser 2 (DLpro, Toptica), which is the one to be locked, is focused onto a fast photodetector (PDA8GS, Thorlabs). The generated beat signal is split and sent to a spectrum analyzer, while the other part is amplified and sent to the OPLL circuit (EVAL-ADF4007, Analog Devices). Based on a reference signal received from a frequency

generator (SMB100A, Rohde Schwarz), the OPLL produces the error signal that is sent to the FALC servo that feeds the corrections to the laser 2.

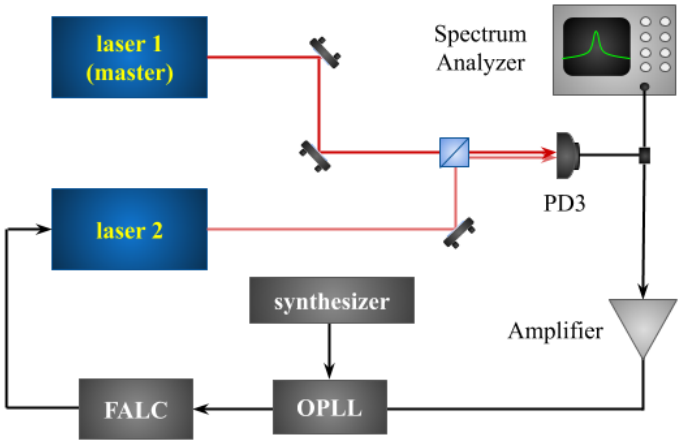

Figure 27 – Schematic representation of an optical phase-locked loop setup

The OPLL signal is a digital phase-frequency-discriminator chip that divides digitally the reference signal by a factor R and the beat signal by a factor N (with a ratio of 8, 16, 32, and 64), and then compares the frequency and phase of both divided signals. The phase lock can thus be implemented for the beat signal of any frequency up to the maximum permitted by the ADF4007 (7.5 GHz), with the reference produced by a MHz-range signal generator.

When the phase difference of the beat and reference signals is small, the OPLL circuit produces a feedback current proportional to it. Otherwise the polarity of the error signal corresponds to the sign of the frequency difference between the two signals (43) . In this way, the capture range of the phase lock circuit is limited only by the modehop free tuning range of the slave laser.

5.3.1 Lattice laser

As mentionned in the previous section, the laser 2 will be used to generate the lattice and probe beams and it is locked to the master laser through the OPLL technique. The characterization of its relative linewidth was performed in the same way for the slave lasers. Figure 28 shows the beat signal between the laser 2 and the master for 10 Hz of BWR. The obtained linewidth is $w = 10.1$ Hz, where the measurement was limited by the BWR. The conclusions made in the discussion of the injection locking also apply to the OPLL lock: The beat note reveals the “relative stability" of the two lasers and, hence, the quality of the PLL. Since the lasers are correlated this is not the linewidth that an independent system, for example, an atomic resonance, would see. The same reasoning as

before applies: Since this correlated linewidth is in the range of Hz, the slave laser inherits the absolute kHz linewidth of the master.

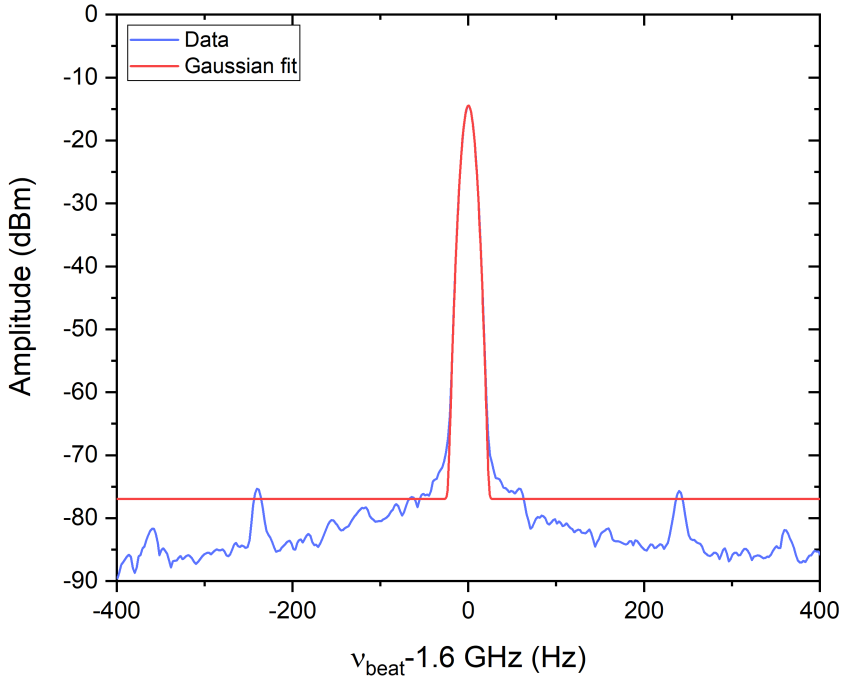

Figure 28 – Beat signal between the laser 2 and the master for a BWR of 10 Hz.

Other tests were performed to evaluate the locking circuit. First, modulation sidebands were applied to the laser frequencies and no discernible impact on the stability of the OPLL was observed. To evaluate the time response of the locking circuit, the error signal was monitored on an oscilloscope and the beat signal with a spectrum analyzer. Then, a 5 kHz square frequency modulation with a deviation of $f_{dev} = 100$ kHz was applied to the synthesizer. We observed a frequency excursion on the spectrum analyzer of 6.4 MHz = $64 \cdot f_{dev}$. The error signal showed a 30 μs long impulse response, which means that the servo can handle a 6.4 MHz jump within 30 μs.

5.4 Reference cavity

For the PDH stabilization, we have to our disposal a high finesse “supercavity" (ATThinFilms) as reference cavity. It consists in a linear cavity of $L = 10$ cm length cavity with a flat mirror ($\rho_1 = \infty$) and a curved one with $\rho_2 = 500$ mm of radius of curvature. The cavity is evacuated down to 1.4×10^{-7} mbar by an ion getter pump and it is maintained at 33 °C by a heating wire consuming $I = 0.63$ A. The temperature is measured by a thermistor whose resistance is kept constant at $R = 7.07$ $k\Omega$. The free

spectral range is $c/2L = 1.5$ GHz. In the following, the experimental characterization of the cavity linewidth and finesse is presented.

5.4.1 Cavity linewidth and finesse

We consider a linear cavity of length L pumped by a laser without any scatterer located inside the cavity. The cavity spectrum is given by the free spectral range δ_{fsr} which is related with the time τ^{-1} for a photon to make a round trip in the cavity

$$\delta_{fsr} \equiv \tau^{-1}, \tag{5.1}$$

where τ^{-1} is given in units of real frequency. Since the field in the cavity decays like $E(t) = E_0 e^{-\kappa t}$, the intensity decay is given by $I(t) = I_0 e^{-2\kappa t}$, where κ is the cavity transmission rate and also the FWHM width of the intensity transmission spectrum (16). Then, we have $\kappa = 1/\tau_\kappa = 1/2\tau_{int}$, where τ_{int} is the intensity decay time. From equation 4.6 we get the following relation for the cavity linewidth

$$\kappa \equiv \frac{1}{2\tau_{int}} = \frac{\pi \delta_{fsr}}{\mathcal{F}}. \tag{5.2}$$

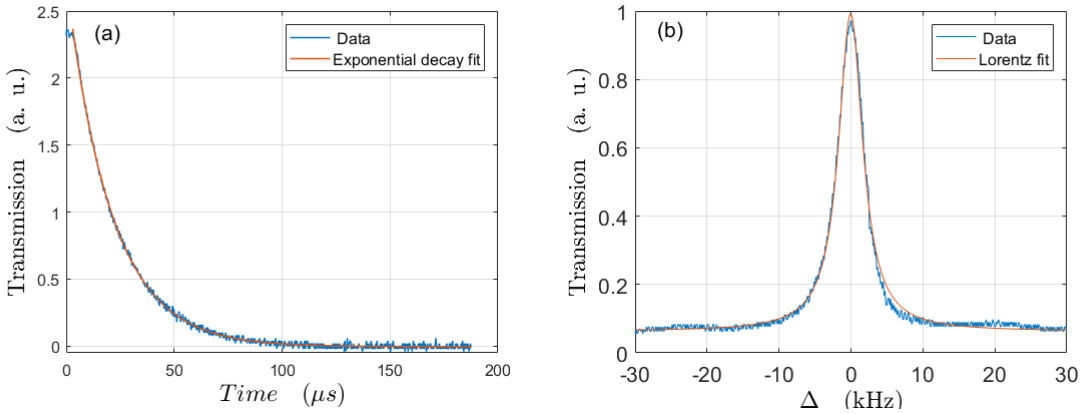

Figure 29 – (a) Cavity ring down measurement. (b) Cavity transmission linewidth.

Figure 29(a) shows a cavity 'ring down' measurement that consists in suddenly turning off the coupled laser and measuring the decay of the transmitted intensity. In order to obtain the intensity decay time τ_{int}, an exponential decay equation written as $y = y_0 A \exp\{-t/\tau_{int}\}$ was used to fit the experimental data. This yielded an intensity decay time $\tau_{int} = (20.76 \pm 0.05)$ μs. With this result and using equation 5.2 we got the cavity linewidth of $\kappa = (2\pi)\ (3.78 \pm 0.32)$ kHz, and the finesse is $\mathcal{F} = (195.66 \pm 0.47) \times 10^3$, while the value specified by the manufacturer of the cavity is $\mathcal{F} = 250 \times 10^3$.

We also directly measured the cavity linewidth by locking the laser 1 to the cavity through the PDH technique and the laser 2 to the first one using the OPLL. Then, the

frequency synthesizer was used to ramp laser 2 across an adjacent mode of the cavity. The transmission spectrum of the super cavity is shown in Figure 29(b), in which a Lorentzian profile of $y = y_0 + \frac{2A}{\pi}\frac{w}{4(x-x_c)^2+w^2}$ was fitted to the data. The light of the resonant master laser (laser 1 is locked to the cavity) leaking through the cavity generates an offset y_0. The w parameter is the FWHM of the resonance profile, therefore, it gives us the cavity linewidth κ. From this fitting we got $\kappa\ (2\pi) = (4.08 \pm 0.03)$ kHz, with a good agreement with the previous measurement.

5.5 Experimental setup overview

As discussed so far, each laser has a specific task in our experiment and each locking method depends on the master laser, which in turn is locked to the reference cavity. Figure 30 shows the block diagram of the locking setup and the tasks of each laser while Figure 31(a) shows an overview of how the locking system is implemented to the experiment while Figure 31(b) shows the frequencies used to accomplish each goal.

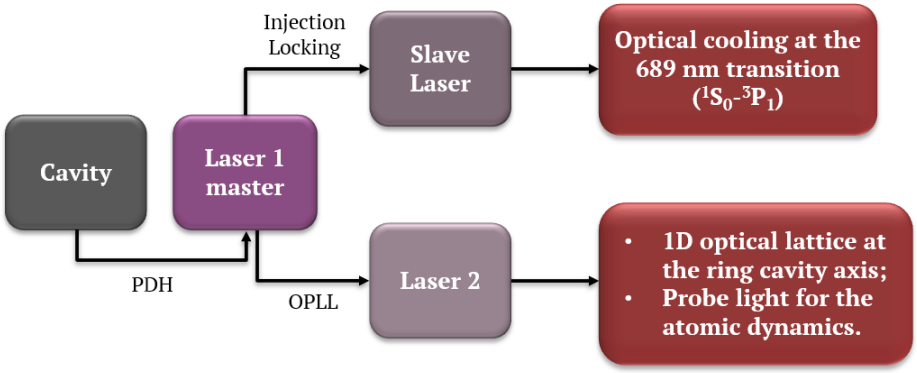

Figure 30 – Block diagram representing the locking scheme and the task of each laser.

To recapitulate, the laser 1 (ν_{l1}) is locked to the reference cavity through the PDH stabilization. This laser is used as a reference laser to frequency stabilize the slave laser through the injection locking method. The slave provides the light for the red MOT ($\nu_{red\ MOT}$). The laser 2 (ν_{l2}) is locked to the laser 1 employing the OPLL stabilization. This laser will provide the light to produce the one-dimensional optical lattice (ν_{BLOCH}) in the axis of the ring cavity, and also the necessary light to probe the atomic dynamics (ν_{CARL}).

The laser 1 (ν_{l1}) is locked to the reference cavity through PDH stabilization, which is detuned from the strontium atomic resonance (ν_{Sr}) by $\Delta = 495$ MHz. To overcome the gap, a fraction of its output light is double passed in the AOM1, in which the light is frequency shifted by $f_{inj} = 400$ MHz. This light is used to stabilize the slave laser by the

injection locking, and its output is frequency shifted by f_{sl} = 80 MHz, and provides the light for red MOT ($\nu_{red\ MOT}$).

The ring cavity has a piezo which allows it to tune its modes to arbitrary positions. One mode is tuned close to the Sr line, such that the atoms can resonantly interact with the cavity, if required. One mode is tuned close to the Sr line, such that the atoms can resonantly interact with the cavity, if required. The next adjacent mode -8.23 GHz is used to operate the optical lattice and the CARL (with orthogonal polarizations).

The laser 2 (ν_{l2}) is used to produce the optical lattice. Since the intercombination light of the red MOT is 7.6 kHz, it is sufficient to lock the laser 2 to the next adjacent resonance (ν_{rng}) whose distance from the resonant mode is given by the ring cavity free spectral range δ_{fsr}^{rng} = 8.23 GHz. The laser 2 is offset locked by 7.625 MHz to the master through the OPLL technique. The AOM3 and AOM4 are used to overcome the frequency difference between the stabilized laser and the ring cavity mode of f_{aom} = -110 MHz. The AOM3 is used to adjust the light responsible for the optical lattice (ν_{BLOCH}) and the AOM4 is used to provide the light that will probe the atomic dynamics. In the future, the ring cavity will be stabilized to the laser 2 through the PDH method.

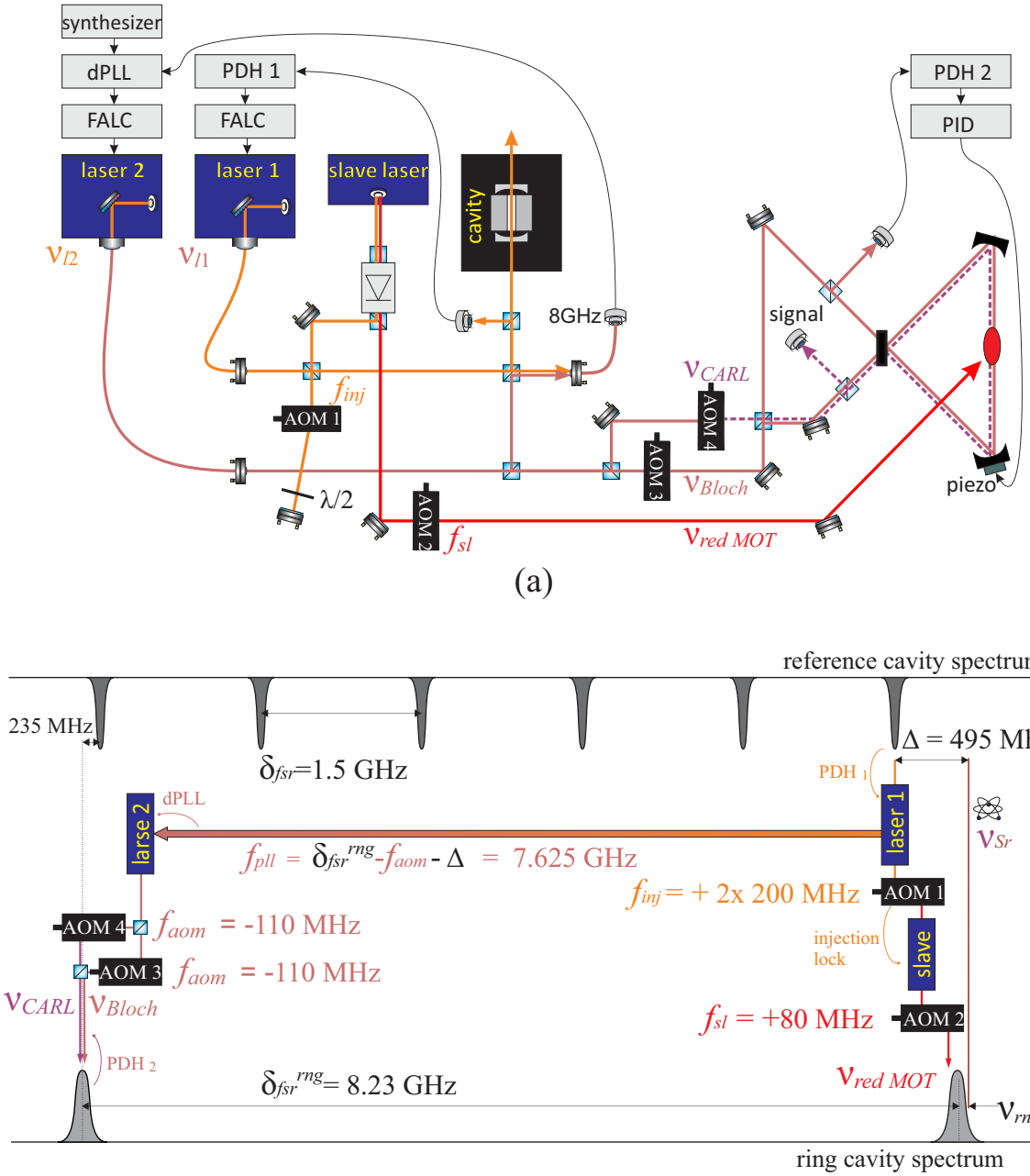

Figure 31 – (a) Overview of the optical setup of the laser locking system and the used of each laser. (b) Locking scheme illustrating the frequency shifts and locking points of the lasers with respect to the supercavity spectrum and the ring cavity spectrum.

6 Conclusion

This project is an important part of an experiment under construction aiming to observe in a non-destructive way the combined dynamics produced by two physical effects: the Bloch oscillations and the collective atomic recoil laser (CARL). To prove this, we choose the atomic species of bosonic strontium isotope ^{88}Sr, which has a narrow intercombination line at 689 nm with a linewidth of 7.6 kHz. As discussed in chapter 3, this should allow us to reach temperatures close to the recoil temperature in a standard MOT.

One of the main advantages of this intercombination line is its optical frequency, in which we can use a diode laser to cool down the atoms in this transition. As presented in chapter 4 the benefits of such lasers are their wide frequency bandwidth, low cost, high efficiency, output power and the possibility of being combined with relatively simple optoelectronic systems for frequency and phase stabilization, leading to a set of versatile and powerful devices that are attractive for use in many existing and novel applications.

However, the narrow linewidth of the atomic transition also brings limitations to the laser system. It requires that the cooling light have a linewidth narrower than the transition. As presented in chapter 4, this can be achieved through the Pound-Drever-Hall stabilization (PDH), in which the master laser is locked to a high finesse cavity, and then used to lock a slave laser by injection locking. After implementing this to our system, a beat signal was performed between the master laser and another independent laser, also locked to a reference cavity through PDH. The measure linewidth of the beat note was $w = 1.13$ kHz. With the master and the slave laser frequency stabilized, the beat signal between both laser was recorded and it was measured a relative linewidth of the order of 20 Hz. Since they are correlated, we infer for the slaved laser an absolute linewidth of the same order as the master ($\sim$ kHz). The slave laser is used to produce the red MOT light, then, it is important that its linewidth is narrower than the intercombination line, as required, which is fulfilled.

Another requirement of the experiment is to produce an optical lattice. Once again, the narrow intercombination line plays a role. Once the linewidth is the order of kHz, it is sufficient to tune the frequency of the optical lattice only a few hundreds of MHz below the atomic resonance. Technically, this was achieved by locking the laser dedicated to this task to the master using an optical phase-locked loop (OPLL). The beat linewidth between the lasers locked via OPLL was measured to be approximately 10 Hz. Again, since the lasers are correlated by the lock, the slaved laser also has a linewidth at the same order as the master.

In the current stage of the experiment, we are able to trap and cool approximately 1×10^6 atoms in the strontium broad transition ($^1S_0 - ^1 P_1$). The next step will be to transfer the atoms to the red MOT and cool them close to the recoil temperature. Then, we will produce the optical lattice directed along the axis of the ring cavity being locked to the laser through PDH stabilization. After that, we will probe the atomic dynamics in a non-destructively way. All the required lasers to achieve this are now set and work properly.

Bibliography

1 KRUSE, D. et al. Observation of lasing mediated by collective atomic recoil. *Phys. Rev. Lett.*, v. 91, n. 18, p. 1–4, 2003. ISSN 10797114. Citado 3 vezes nas páginas 7, 14, and 15.

2 SAMOYLOVA, M. et al. Mode-locked Bloch oscillations in a ring cavity. *Laser Phys. Lett.*, v. 11, n. 12, 2014. ISSN 1612202X. Citado 7 vezes nas páginas 7, 11, 12, 13, 17, 18, and 19.

3 PEDEN, B. et al. Nondestructive cavity qed probe of bloch oscillations in a gas of ultracold atoms. *Physical Review A*, v. 80, p. 043803, 2009. Citado na página 11.

4 SAMOYLOVA, M. et al. Synchronization of bloch oscillations by a ring cavity. *Optics Express*, v. 23, p. 14823–14835, 2015. Citado na página 11.

5 KEßLER, H. et al. In situ observation of optomechanical bloch oscillations in an optical cavity. *New Journal of Physics*, v. 18, p. 102001, 2016. Citado na página 11.

6 GUO, P. R. B. J.; B.DUBETSKY. Recoil-induced resonances in nonlinear spectroscopy. *Physical Review A*, v. 46, n. 3, p. 102001, 1992. Citado na página 11.

7 STENGER, J. et al. Bragg spectroscopy of a bose-einstein condensate. *Physical Review Letter*, v. 82, n. 23, p. 4569, 1999. Citado na página 11.

8 ANDREWS, M. R. et al. Direct, nondestructive observation of a bose condensate. *Science*, v. 273, p. 24, 1996. Citado na página 11.

9 GERICKE, T. et al. High-resolution scanning electron microscopy of an ultracold quantum gas. *Nature Physics*, v. 4, p. 949, 2008. Citado na página 11.

10 SLAMA, S. et al. Superradiant rayleigh scattering and collective atomic recoil lasing in a ring cavit. *Phys. Rev. Lett.*, v. 98, p. 203601, 2007. Citado na página 11.

11 BUX, S. et al. Cavity-controlled collective scattering at the recoil limit. *Phys. Rev. Lett.*, v. 106, p. 203601, 2011. Citado na página 11.

12 BERRADA, T. et al. Integrated Mach-Zehnder interferometer for Bose-Einstein condensates. *Nat. Commun.*, v. 4, n. May, p. 1–8, 2013. ISSN 20411723. Citado na página 12.

13 PETTERS, A.; CHUNG, K.; CHU, S. Measurement of gravitational acceleration by dropping atoms. *Nature*, v. 400, 1999. Citado na página 12.

14 PETERS, A.; CHUNG, K. Y.; CHU, S. High-precision gravity measurements using atom interferometry. *Metrologia*, v. 38, p. 25–61, 2001. Citado na página 12.

15 BONIFACIO, R.; De Salvo, L. Collective atomic recoil laser (CARL) optical gain without inversion by collective atomic recoil and self-bunching of two-level atoms. *Nucl. Inst. Methods Phys. Res. A*, v. 341, n. 1-3, p. 360–362, 1994. ISSN 01689002. Citado na página 12.

16 COURTEILLE, P. W. *Quantum Mechanics applied to Atoms and Light*. [S.l.], 2020. Citado 4 vezes nas páginas 14, 16, 24, and 56.

17 BLOCH, F. Bemerkung zur Elektronentheorie des Ferromagnetismus und der elektrischen Leitfähigkeit. *Zeitschrift für Phys.*, v. 57, n. 7-8, p. 545–555, 1929. ISSN 14346001. Citado na página 15.

18 ALL, K. L. et. Observation of bloch oscillations in a semiconductor superlattice. *Solid State Communications*, v. 84, n. 10, p. 943–946, 1992. Citado na página 15.

19 FERRARI, G. et al. Long-lived bloch oscillations with bosonic Sr atoms and application to gravity measurement at the micrometer scale. *Phys. Rev. Lett.*, v. 97, n. 6, p. 1–4, 2006. ISSN 00319007. Citado 2 vezes nas páginas 15 and 17.

20 PEIK, E. et al. Bloch oscillations of atoms, adiabatic rapid passage, and monokinetic atomic beams. *Phys. Rev. A - At. Mol. Opt. Phys.*, v. 55, n. 4, p. 2989–3001, 1997. ISSN 10941622. Citado 2 vezes nas páginas 16 and 17.

21 STECK, D. A. *Quantum and Atom Optics*. 0.13.1. ed. [S.l.], 2020. Citado 2 vezes nas páginas 20 and 21.

22 METCALF, H. J.; STRATEN, P. van der. *Laser Cooling and Trapping*. [S.l.]: Springer Science, 1999. Citado na página 20.

23 PHILLIPS, W. D. Optical molasses. *CPEM Dig. (Conference Precis. Electromagn. Meas.*, v. 6, n. 11, p. 4, 1990. ISSN 05891485. Citado 2 vezes nas páginas 21 and 23.

24 DALIBARD, J.; COHEN-TANNOUDJI, C. Laser cooling below the Doppler limit by polarization gradients: simple theoretical models. *J. Opt. Soc. Am. B*, v. 6, n. 11, p. 2023, 1989. ISSN 0740-3224. Citado na página 24.

25 BLOOM, B. J. et al. An optical lattice clock with accuracy and stability at the 1018 level. *Nature*, v. 506, p. 71–75, 2014. Citado na página 26.

26 FERRARI, G. et al. Long-lived bloch oscillations with bosonic sr atoms and application to gravity measurement at the micrometer scale. *Phys. Rev. Lett.*, v. 97, p. 060402, 2008. Citado na página 27.

27 ARMIJOS, M. A. M. *Construction of an experiment providing cold strontium atoms for atomic interferometry in a ring cavity*. Dissertação (Master Thesis) — Universidade de São Paulo, 2020. Citado na página 29.

28 CHOI, Y. et al. Direct measurement of loading and loss rates in a magneto-optical trap with atom-number feedback. *Phys. Rev. A - At. Mol. Opt. Phys.*, v. 76, n. 1, p. 1–7, 2007. ISSN 10502947. Citado na página 30.

29 KETTERLE, W.; DURFEE, D. S.; STAMPER-KURN, D. M. *Making, probing and understanding Bose-Einstein condensates*. 1999. Disponível em: <http://arxiv.org/abs/cond-mat/9904034>. Citado na página 32.

30 LOFTUS, T. H. et al. Narrow line cooling and momentum-space crystals. *Physics Review A*, n. 70, 2004. Citado na página 33.

31 DING, R. *Narrow Line Cooling of* ^{84}Sr. Dissertação (Master Thesis) — Rice University, 2016. Citado na página 34.

32 WIEMAN, C. E.; HOLLBERG, L. Using diode lasers for atomic physics. *Rev. Sci. Instrum.*, v. 62, n. 1, p. 1–20, 1991. ISSN 10897623. Citado na página 36.

33 PENG, Q. et al. Lasers in medicine. *Reports Prog. Phys.*, v. 71, n. 5, 2008. ISSN 00344885. Citado na página 36.

34 BLACK, E. D. An introduction to Pound–Drever–Hall laser frequency stabilization. *Am. J. Phys.*, v. 69, n. 1, p. 79–87, 2001. ISSN 0002-9505. Citado 4 vezes nas páginas 37, 39, 40, and 42.

35 COURTEILLE, P. W. *Electrodynamics - Electricity, Magnetism and Radiation*. 2020. Disponível em: <http://www.ifsc.usp.br/~strontium/>. Citado na página 37.

36 LIU, Z.; SLAVIK, R. Optical Injection Locking: From Principle to Applications. *J. Light. Technol.*, IEEE, v. 38, n. 1, p. 43–59, 2020. ISSN 15582213. Citado 2 vezes nas páginas 43 and 44.

37 Lau, E. K.; Wong, L. J.; Wu, M. C. Enhanced modulation characteristics of optical injection-locked lasers: A tutorial. *IEEE Journal of Selected Topics in Quantum Electronics*, v. 15, n. 3, p. 618–633, 2009. Citado na página 44.

38 STEPHENS, D. R. *Phase-Locked Loops for Wireless Communications_ Digital, Analog and Optical Implementations*. [S.l.: s.n.], 2002. ISBN 0-306-47314-3. Citado na página 46.

39 SATYAN, N. *Optoelectronic Control of the Phase and Frequency of Semiconductor Lasers*. 2014 p. Tese (Doutorado), 2011. Disponível em: <http://resolver.caltech.edu/CaltechTHESIS:04292011-221312708>. Citado 2 vezes nas páginas 46 and 47.

40 ELLIOTT, D. S.; ROY, R.; SMITH, S. J. Extracavity laser band-shape and bandwidth modification. *Phys. Rev. A*, American Physical Society, v. 26, p. 12–18, Jul 1982. Disponível em: <https://link.aps.org/doi/10.1103/PhysRevA.26.12>. Citado na página 50.

41 BOTINEAU, J.; STOLEN, R. H. Effect of polarization on spectral broadening in optical fibers. *J. Opt. Soc. Am.*, OSA, v. 72, n. 12, p. 1592–1596, Dec 1982. Citado na página 50.

42 KATORI, H. et al. Magneto-optical trapping and cooling of strontium atoms down to the photon recoil temperature. *Phys. Rev. Lett.*, v. 82, p. 1117–1119, 1999. Citado na página 51.

43 APPEL, J.; MACRAE, A.; LVOVSKY, A. I. A versatile digital GHz phase lock for external cavity diode lasers. *Meas. Sci. Technol.*, v. 20, n. 5, 2009. ISSN 09570233. Citado 2 vezes nas páginas 53 and 54.